CONCEPTUAL DESIGN REPORT

Scientific Instrument Single Particles, Clusters, and Biomolecules (SPB)

January 2012

A.P. Mancuso

for Scientific Instrument SPB (WP84)

at the European XFEL

European XFEL

Contents

1 Overview and summary

This chapter describes the objective, goals, background, rationale, and classes of experiments for the Single Particles, Clusters, and Biomolecules (SPB) instrument.

Objective

The Single Particles, Clusters, and Biomolecules (SPB) instrument aims to image single particles by exploiting coherent diffraction imaging and associated methods using hard X-ray free-electron laser (FEL) radiation. In particular, the SPB instrument's goals have been discussed with the coherent imaging community, and are recorded in the document titled "International workshop on science with and instrumentation for ultrafast coherent diffraction imaging of Single Particles, clusters and Biomolecules (SPB) at the European XFEL" [1].

Specifically, the SPB instrument will be designed to image single particles, which explicitly includes:

- Isolated, non-crystalline biomolecules

- Nanocrystals of biomolecules

- Atomic clusters

- Other isolated, single particles, in particular those of a "reproducible" nature

Furthermore, the SPB instrument aims to investigate the structure of these systems, as a function of time, through the use of so-called "pump-probe" measurements, where an optical laser excites a sample and the FEL probes it some delay time later (for example, see [2]).

Goals

The goal of the SPB instrument is to be a world-leading instrument, making possible the science listed in "Objective" on page 4. The goal of this document is to outline the conceptual design of the SPB instrument, one of the initial six instruments to be installed and operated at the future European XFEL facility in Hamburg and Schenefeld, Germany [3]. This includes descriptions of the major subsystems of the SPB instrument, including the instrument's optics, the sample injection environment, the detector(s) required, and the necessary diagnostics in the end station. This document is a conceptual design report, and, as such, does not include all the details required to construct the instrument. A more detailed technical design report (TDR) will be produced subsequent to this document.

Approach

One of the key properties of the conceptual design is the balance between a clear, realistic design and the flexibility required to adapt to the changing needs of single particle imaging, which is rapidly developing due to the recent commencement of operation of hard X-ray FELs in the USA [4] and in Japan [5]. Parts of this document propose more than one solution to the instrument design. In particular, this occurs when it is technically not challenging to maintain flexibility in the design (e.g. interchangeable, low-cost optics) or where a given, available technology is able to solve only a subset of the problems above and another technology better solves another subset of problems (e.g. different focusing optics for single particle imaging compared with nanocrystallography).

Background and rationale

This document is primarily informed by the user workshop entitled "International workshop on science with and instrumentation for ultrafast coherent diffraction imaging of Single Particles, Clusters and Biomolecules (SPB) at the European XFEL" held in Uppsala, Sweden, in November 2008.

The workshop's content and purpose can be summarized by the following observation:

> *"The study of structural properties of single particles, clusters, and bio-molecules (SPB) using coherent X-ray diffraction by particles in the gas phase is one of the prioritized areas of science for the upcoming European XFEL facility. These experiments will be relevant to several areas of science, reaching from materials and nano-sciences to biology. The workshop brought together scientists interested in experiments using the SPB instrument at the European XFEL facility to review the science planned with this instrument, to discuss the requirements to the X-ray FEL beam delivery, and to initiate activities and collaborations on instrumentation and facilities needed at this photon end station."* [1]

The full program of the workshop (including copies of presenters' slides) can be found on the SPB Workshop 2008 webpage:

http://www.xfel.eu/events/workshops/2008/spb_workshop_2008/

This page also includes the subsequent report summarizing the workshop's findings [1].

Single particle imaging becomes feasible due to the unprecedented photon flux and spatial coherence of FEL sources. The highest X-ray flux available (hence FEL) is needed to be able to measure and interpret the still very weak signal one expects from single particles. Furthermore, many shots or frames of data are required for successful interpretation of that data [6] [7]. On this front, the European XFEL has a unique advantage due to the unprecedented pulse rate produced by the superconducting accelerator technology used. With access to orders of magnitude more pulses compared to other facilities around the world, the SPB instrument, it is hoped, will explore science that is

broader than that currently possible at existing FEL sources, for example by investigating the dynamics of these samples in the pump-probe mode with many different delay times or exploring the breadth of conformations present in a single molecule.

A variety of methods for structure determination will be available at the SPB instrument, including (but not limited to) single particle imaging and nanocrystallography. This will allow the investigation of structural biology in samples that are impossible to study without FEL radiation. Furthermore, the SPB instrument will provide the opportunity to explore the fundamental physics of intense X-ray photon-matter interactions through the use of single- or few-element controlled samples, such as atomic clusters.

Three key classes of experiments

One can group the proposed experiments to be performed at the SPB instrument into three key classes, based on (i) the sample to be investigated, (ii) the requirements on the beam to investigate a given type of sample, and (iii) the expected signal scattered from the sample after interaction with the European XFEL beam.

Single particle imaging of biomolecules

One class of interest is single biomolecules and macromolecular complexes. These samples are typically some tens of nanometers in their longest dimension and are composed of predominantly carbon, nitrogen, and oxygen. The X-ray scattering from such an object is, as expected, very weak; as such, maximizing the single pulse photon flux delivered to the sample is critical for this class of experiments. This requirement imposes the constraint that the X-ray optics used to focus and deliver the FEL beam to the sample must be highly transmissive, with the largest fraction of the beam being delivered to the interaction region in a focal spot comparable to (≈ 2–3 x) the size of the sample. Even given the ultrabright nature of the XFEL pulses, the signal expected from such a sample at the detector may be as small as some few tens of photons across an entire 2D detector [6] [7], placing stringent requirements of single photon sensitivity on the 2D detector used.

Furthermore, as the knowledge of atomic positions is of considerable importance for the broadest success of single molecule imaging, the instrument geometry should accommodate the collection of scattering data down to 2 Å resolution or better [8] [9].

Also critical is the transverse intensity and wavefront distribution of the beam incident on the sample. Variations in the incident beam's structure on the scale of the features to be imaged will themselves contribute to the measured signal and final image, unless they are themselves characterized and accounted for in the imaging process [10] [11]. This places stringent requirements on the X-ray optics to minimize intensity and wavefront structure, due to apertures and optical aberrations, as well as on the X-ray diagnostics to measure and characterize any such variations.

The summary requirements to this class of experiment are:

- Maximum number of photons delivered to the sample, in a spot size comparable with the sample size

- Flat, uniform, or characterizable wavefront in the focal plane

- Single photon sensitive detector (elaborated in Chapter 9, "Detector system", on page 65)

- Means to deliver particles to the interaction region at a rate that matches the X-ray pulse rate

- Resolutions better than 2 Å

Nanocrystallography

Samples for nanocrystallography are, as the name suggest, crystalline. To date, samples down to hundreds of nanometers in size have been investigated [12]. As for the biomolecules case described in "Single particle imaging of biomolecules" on page 7, it is desirable to maximize the scattered signal by using high transmission optics and by matching the focal size to the sample size. In the simplest nanocrystallographic analysis, a highly controlled or characterized wavefield is not required, and the crystallographic phase problem is solved using a generalization of traditional crystallographic techniques [13]. Accordingly, as in conventional crystallography, there is a

need for many pixels in the detector to accurately determine the centre of each Bragg peak measured.

Beyond that, a further analysis of nanocrystallographic data, which utilizes the coherent diffraction information around a Bragg peak [14], has the same requirements on the incident wavefield as the single particle case above, namely a flat or well-characterized intensity and wavefront distribution. However, unlike for the investigation of weakly scattering single biomolecules, the analysis of the data around the Bragg peaks requires a large dynamic range in the detector. The signal around a Bragg peak quickly decreases with distance from the centre of the peak.

The summary requirements to this class of experiment are:

- Maximum number of photons delivered to the sample, in a spot size comparable with the crystal size

- High number of pixels in the detector for accurate centroid determination of Bragg peaks

- For the most thorough analysis, a flat, uniform, or characterizable wavefront in the focal plane

- High dynamic range in the detector

- Wavelength tunability around elemental absorption edges

- Nanocrystal delivery or mounting system that replenishes samples at a rate that matches the X-ray pulse rate

- Resolutions better than 2 Å
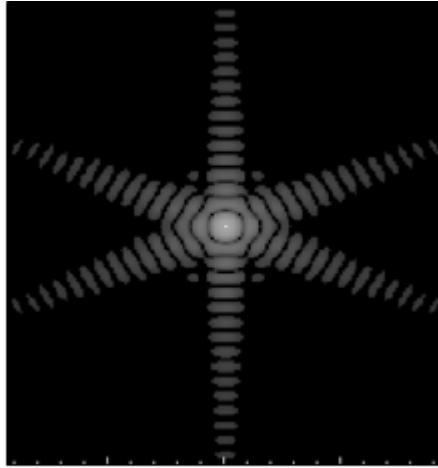
Figure 1. *A simulated diffraction pattern around a Bragg peak produced by an icosahedral-shaped crystal. The signal shown here (on a log scale) spans more than three orders of magnitude. Weaker signal from the simulation has been suppressed by a modelled noise-floor.*

Larger single particles

Larger biological samples, such as small cells, organelles, or viruses, or more strongly scattering samples, such as materials science samples composed of heavier elements, present a third category of experiments that is envisaged for the SPB instrument. These samples will create a continuous diffraction pattern that spans many orders of magnitude in its dynamic range. Here the beam requirements are similar to the most stringent cases described above, except the required focal spots are likely to be larger. The control or characterization of the incident intensity and wavefront is also essential for a thorough analysis in these cases.

The demands on detection are most pertinent in the requirement of a high dynamic range, as the scattered signal falls off rapidly with angle in the diffraction pattern. Ultimately, this effect limits the resolution of any reconstruction. Subunits of cells, such as the Nuclear Pore Complex [15], can be hundreds of nanometers in size. Useful resolutions are then on the single-digit nanometer range, giving access to hundreds of resolution elements across these type of sub-cellular assemblies. As the scattering signal decreases proportionally to the fourth power of feature size, the desired number of resolution elements places a direct requirement on the dynamic range of the detector or detector system, ideally to span the number of resolution elements to the fourth power.

The summary requirements to this class of experiment are:

■ Maximum number of photons delivered to the sample, in a spot size comparable with the sample size

■ Flat, uniform, or characterizable wavefront in the focal plane

■ High dynamic range in the detector

■ Sample delivery or mounting system that may depend on the quantity of samples

■ Resolutions in the single-digit nanometer range
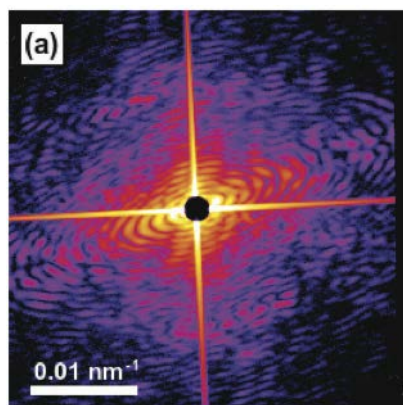
Figure 2. An example of a coherent diffraction pattern from a single-celled organism with strong signal spanning orders of magnitude of dynamic range. Figure originally published in A.P. Mancuso et al., New J. Phys., 12, 035003 (2010).

Other coherent imaging techniques

There exist a plethora of other coherent imaging techniques including (but not limited to) in-line holography [16] [17], Fourier transform holography [18], Fresnel Coherent Diffractive Imaging (FCDI) [19], phase-diverse imaging methods [20], and techniques that account for partial transverse [21] and temporal [22] coherence. Furthermore, scattering experiments, including solution scattering and powder diffraction, are also viable options. These methods are also included in the broader mission and application of the SPB instrument, but are not considered in detail in this document.

2   Advisory review team

This chapter describes the role of the advisory review team (ART) and lists its members.

Role

The ART is a panel of experts in diverse matters related to single particle imaging. The ART provides advice on the design of the SPB instrument and also provides a review function to give feedback on the SPB design and implementation.

The ART is expected to review the instrument's conceptual and technical design as well as to provide advice and feedback continuously until the instrument's final delivery.

Members

Prof. Dr Franz Pfeiffer (Chair)
Physics Department (E17) and Institute of Medical Engineering (IMETUM)
Technische Universität München
James-Franck-Straße
85748 Garching
Germany
Phone: +49 89 289 12552
Fax: +49 89 289 12548
franz.pfeiffer@ph.tum.de

Dr Sebastien Boutet

CXI Instrument Scientist

LCLS, SLAC Accelerator Laboratory

2575 Sand Hill Rd

Menlo Park, CA 95205

USA

Phone: +1 650 926 8676

Fax: +1 650 926 3600

sboutet@slac.stanford.edu

Dr Garth Williams

CXI Instrument Scientist

LCLS, SLAC Accelerator Laboratory

2575 Sand Hill Rd

Menlo Park, CA 95205

USA

Phone: +1 650 926 2682

Fax: +1 650 926 3600

gjwillms@slac.stanford.edu

Dr Anton Barty

Centre for Free-Electron Laser Science

Deutsches Elektronen-Synchrotron (DESY)

Notkestraße 85

D-22607 Hamburg

Germany

Phone: +49 40 8998 5783

Fax: +49 40 8998 1958

anton.barty@desy.de

Dr Dan DePonte

Centre for Free-Electron Laser Science

Deutsches Elektronen-Synchrotron (DESY)

Notkestraße 85

D-22607 Hamburg

Germany

Phone: +49 40 8998 5784

Fax: +49 40 8998 1958

daniel.deponte@desy.de

Prof. Dr Ilme Schlichting

Director, Dept. of Biomolecular Mechanisms

Max Planck Institute for Medical Research

Jahnstraße 29

69120 Heidelberg

Germany

Phone: +49 6221 486-500

Fax: +49 6221 486-351

ilme.schlichting@mpimf-heidelberg.mpg.de

Prof. Dr Victor Lamzin

Deputy Head of Outstation and Senior Scientist

European Molecular Biology Laboratory (EMBL) Hamburg

Deutsches Elektronen-Synchrotron (DESY)

Notkestraße 85

22603 Hamburg

Germany

Phone: +49 40 8990 2121

Fax: +49 40 8990 2149

victor@embl-hamburg.de

3   Note on contributions

Many people have contributed to this conceptual design report. A number of experts have contributed significantly to different chapters through text, diagrams, or otherwise.

These experts are:

Expert	Area
Harald Sinn, European XFEL	Optical Layout
Liubov Samoylova, European XFEL	X-ray Focus Simulation
Max Lederer, European XFEL	Pump Laser
Chris Youngman, European XFEL	Data Acquisition, Management, and Analysis
Krzysztof Wrona, European XFEL	Data Management
Burkhard Heisen, European XFEL	Scientific Computing
Markus Kuster, European XFEL	Detectors
Julian Becker, DESY	Experiment Modelling Program: Detector Effects
Heinz Graafsma, DESY	Experiment Modelling Program: Detector Effects
Dan DePonte, Centre for Free-Electron Laser Science, DESY	Sample Injection Technology
Zoltan Jurek, Centre for Free-Electron Laser Science, DESY	Photon–Matter Interaction Simulation
Beata Ziaja, Centre for Free-Electron Laser Science, DESY	Photon–Matter Interaction Simulation

The above experts are thanked for their exemplary contributions. Any errors remaining in this document are entirely the responsibility of the author.

Valuable discussions were held with a variety of members of the single particle imaging community and the FEL community. Sébastien Boutet and Garth Williams of the Coherent X-Ray Imaging (CXI) instrument at LCLS, SLAC National Accelerator Laboratory, USA, provided a wealth of advice and

information based on their experience at CXI to date. Anton Barty and Henry Chapman have generously provided practical insights into methods of data collection utilized in recent single particle imaging and nanocrystallography experiments performed by the team of the Centre for Free-Electron Laser Science at DESY in Hamburg, Germany. Mike Pivovaroff and Stefan Hau-Riege of Lawrence Livermore National Laboratory provided valuable correspondence on the feasibility of Silicon Carbide-on-metal mirror bilayer coatings for FEL applications. Duane Loh of SLAC provided clear insight into structure determination methods for the 3D imaging of very weakly scattering specimens. Oleg Chubar, Alexey Buzmakov, and Liubov Samoylova are responsible for the cross-platform, wave-optics software, SRWLib, used to simulate the focal properties of the SPB instrument. Evgeny Schneidmiller and Michael Yurkov provided simulations of the FEL photon beam properties for a variety of operating parameters. Alke Meents of DESY, Hamburg, generously provided valuable insights into X-ray optics and instrumentation, and Janos Hajdu provided background on the nature of the biological samples the SPB instrument aims to investigate.

Valuable feedback on this text was provided by Thomas Tschentscher of the European XFEL and as well as Massimo Altarelli, Andreas Schwarz, and Serguei Molodtsov, all members of the European XFEL Management Board. Michael Meyer, Anders Madsen, and Christian Bressler, all leading scientists at the European XFEL, are also thanked for their feedback on the conceptual design and layout. Andrew Aquila and Klaus Giewekemeyer provided valuable suggestions on this document's contents and expression. Kurt Ament assisted enormously with the presentation, layout, and editing.

The ART and the Scientific Advisory Committee of the European XFEL have contributed review comments and insights to the next stage of design of the SPB instrument. Their diligent work in providing advice and feedback is also thoroughly appreciated.

4 Photon beam properties

This chapter describes the radiation from the SASE1 undulator and the experiment modelling program that, amongst other goals, aims to model the photon beam properties at the sample.

Radiation from the SASE1 undulator

The SPB instrument will be located in the centre beamline after the SASE1 undulator of the European XFEL, as shown in Figure 3.
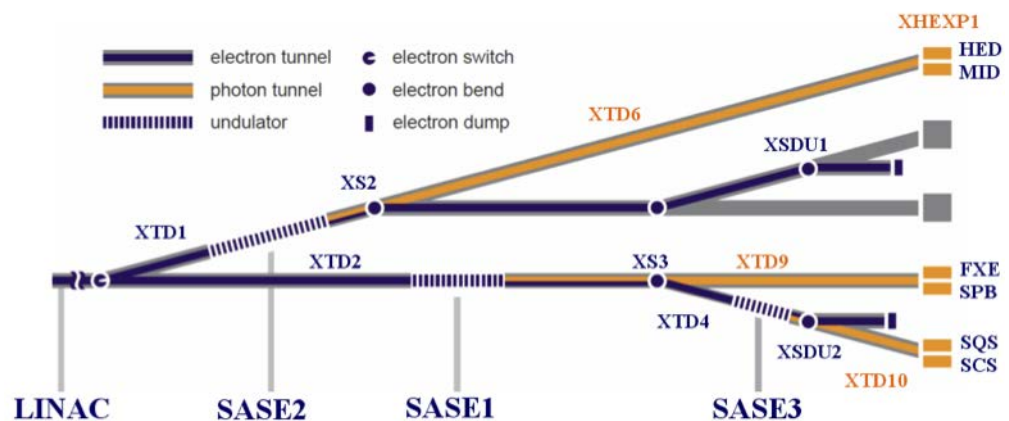
Figure 3. *Layout of the European XFEL accelerator, undulator, and X-ray beam transport systems. Note that the SPB instrument is located after the SASE1 undulator. Figure sourced from [23].*

Table 1, taken from [24], contains calculated values for properties of the radiation produced by this undulator. We note that, in general, the beam is highly spatially coherent, with the degree of coherence reducing for harder energy X-rays or higher bunch charge in the accelerator (that is, higher photon flux). The source size is expected to be between about 30 and 50 µm FWHM across a range of different parameters.

Table 1. *Photon beam parameters for SASE1 as a function of machine operating parameters for some photon energies in the SPB instrument's range of operation, from 3 to 16 keV. Note well that these parameters are given for operation at saturation. The pulse energy, for example, is likely to increase for operation in the oversaturated regime.*

Parameter	Unit	Value								
Photon energy	keV	7.75			12.4			15.5		
Radiation wavelength	nm	0.16			0.10			0.08		
Electron energy	GeV	14			14			14		
Bunch charge	nC	0.02	0.25	1	0.02	0.25	1	0.02	0.25	1
Peak power	GW	46	37	24	35	24	12	29	15	9
Average power	W	2	23	69	2	15	34	1	9	27
Source size (FWHM)	µm	31	39	46	29	37	49	29	35	54
S. divergence (FWHM)	µrad	2.8	2.3	1.9	1.9	1.5	1.3	1.5	1.3	1.0
Spectral bandwidth	1E-3	2.3	1.9	1.4	1.9	1.4	1.0	1.6	1.3	0.8
Coherence time	fs	0.16	0.20	0.27	0.13	0.17	0.23	0.12	0.15	0.23
Coherence degree		0.96	0.96	0.91	0.95	0.91	0.71	0.96	0.84	0.57
Photons/pulse	1E11	0.6	7.0	20.7	0.3	2.8	6.4	0.2	1.4	4.0
Pulse energy	µJ	76	864	2570	58	549	1260	49	347	991
Peak brilliance	1E33*	2.38	2.41	1.96	3.54	3.17	1.6	4.26	2.46	1.6
Average brilliance	1E23*	1.1	15.1	56.8	1.6	19.9	46.4	1.9	15.5	46.2

* In units of photons/(mm^2 mrad^2 0.1% bandwidth s)

In Table 2, again from [24], we see the desired operating range of the SPB instrument, its proposed range of beam size as requested at the SPB workshop [1] and its proposed bandwidth. The proposed bandwidth to be used is the natural bandwidth of the FEL ($\Delta E/E \approx 1 \times 10^{-3}$). This document outlines the addition of a monochromator in Chapter 5, "Optical layout", on page 27.

Table 2. Fundamental operating parameters of the SPB instrument, as discussed at the SPB workshop [1] and modified from that tabulated in [24].

Scientific instrument	Photon energy [kev]	Bandwidth $\Delta\omega/\omega$	Beam size [µm]	Special optics
SPB	3–16	natural	0.1–10; < 1 000	Extreme focusing

The European XFEL is designed to be capable of producing pulses of less than 10 fs in duration for sub-100 pC bunch charges. In order to utilise the "diffract-and-destroy" principle, it is expected that pulse durations below 10 fs are necessary [25] [26]. For other applications, such as nanocrystallography, these duration constraints appear to be significantly reduced, with pulses of hundreds of femtoseconds duration viable in some cases [27]. However, for single particles and nanocrystals, the key parameter to maximize is pulse intensity, achieved with the highest pulse power. A peak power of 46 GW focused to a 0.1 micron diameter spot would give a maximum of 4.6×10^{20} W/cm^2.

Table 3. Pulse duration as a function of bunch charge [24]

Parameter	Unit	Value				
Bunch charge	pC	20	100	250	500	1 000
Pulse duration (FWHM)	fs	2	9	23	43	107

Experiment modelling program

This section describes the goals, participants, and progress of the experiment modelling program, as well as the related X-ray optics and propagation code and photon–matter interaction simulation.

Goals

As modelling the FEL operating parameters is essential to inform appropriate planning of the facility, it is also desirable to model simplified instances of experiments that are expected to be performed in the end stations. This informs the technical design of the instruments, helps understand potential bottlenecks, and ultimately allows us to possess a tool capable of evaluating expected signal levels for designing and understanding the feasibility of proposed experiments.

A modelling program for SPB has been started that aims to achieve these goals through:

- Simulating the different stages of the experiment, starting with the generation of the radiation

- Modeling its transport to the interaction region

- Modeling the photon-matter interaction between the FEL beam and a model sample

- Propagating the radiation to the 2D detector system and its measurement in that detector system

- Interpreting the measured data

This ambitious program is modular in design, with modules focusing on each of the above stages of the overall system (see Figure 4). This allows the project participants to work independently on each of the stages listed above, which can then be combined into a complete start-to-end (S2E) simulation to model an entire (albeit simplified) experiment. Of particular relevance here will be its usefulness in verifying this conceptual design and informing the subsequent technical design of the SPB instrument.

Physically, the pulses propagate through the instrument in the following steps:

Source → Optics → Sample → Photon/Matter Interaction → Propagation to Detector

→ Measurement at Detector → Analysis and Reconstruction → Sample Structure
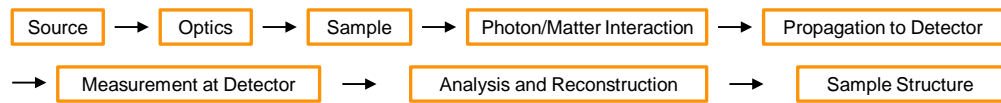
The project is organized into the following modules:

Source → Optics → Photon/Matter Interaction → Detector → Analysis

Figure 4. *Organization of the start-to-end (S2E) simulation program*

Participants

A variety of collaborators from different institutions in the Hamburg area are taking part in each of the S2E's modules and are listed in Table 4.

Table 4. *List of participants (to November 2011) in the start-to-end (S2E) simulation program*

| Name	Organization	Role
Liubov Samoylova	European XFEL	X-ray optics, propagation code
Beata Ziaja	CFEL	Photon–Matter Interaction Simulation
Zoltan Jurek	CFEL	Photon–Matter Interaction Simulation
Markus Kuster	European XFEL	Detector Effects
Julian Becker	DESY	Detector Effects
Heinz Graafsma	DESY	Detector Effects
Mikhail Yurkov	DESY	Source photon field simulations
Evgeny Schneidmiller	DESY	Source photon field simulations
Krzysztof Wrona	European XFEL	Scientific Computing, Image Reconstruction
Burkhard Heisen	European XFEL	Scientific Computing, Image Reconstruction
Adrian Mancuso	European XFEL	Coordinator, Image Reconstruction
Thomas Tschentscher	European XFEL	Director responsible for optics and SPB

Progress

The key progress to date has been defining the modules and their corresponding responsible partners. At present, each module has at least one functioning simulation code that could contribute to the overall goals of the project. The technical interfaces between each module are, at the time of writing, being defined to allow the efficient communication of information from each module to its corresponding downstream recipient. The progress in the individual components is described below.

X-ray optics and propagation code

The X-ray optics and propagation code has been thoroughly utilized in the "Optical Layout" section later in this document to simulate transverse and longitudinal beam profiles after passing through the SPB optics, for different beam parameters. This code [28], designed for XFEL applications, presently assumes the beam is fully spatially coherent, which is a very good approximation in practice for realistic parameters of an FEL beam [29] [30].

Photon–matter interaction simulation

The CFEL theory team has performed an initial simulation using a human three-phosphoglycerate kinase molecule (atomic coordinates from the pdb database, pdb id: 2YBE). This molecule consists of 3 240 atoms in a volume of approximately 50 x 50 x 70 Å^3. As the first step of the project, the team of the Photon-Matter Interaction module calculated the structure factor F of a static molecule, e.g. without any radiation damage within the structure. The atomic form factors were calculated using the XATOM package [31]. The scattering data were calculated on a grid in reciprocal space. The minimum density of grid points is defined by the size of the molecule, but we chose a grid with six times more points (in each linear direction) than that required by Shannon sampling, to have a finer sampling appropriate for the imaging module of the project. The size of the volume in reciprocal space was defined by the desired resolution of 2 Å. According to these values, the total number of grid points is around 100 million resulting in 16 GB of data in HDF5 format [32]. A visualization of this data is shown in Figure 5.
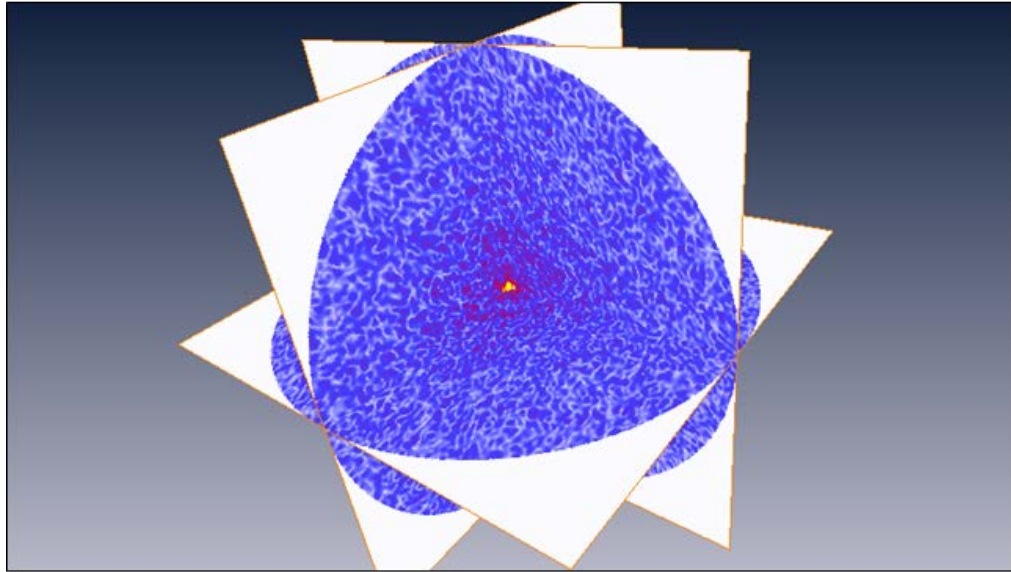
Figure 5. *Visualization of the 3D simulated diffraction data from a three-phosphoglycerate kinase molecule.*

Detector effects

The detector effects team has developed a simulation tool, called HPAD Output Response Function Simulator (HORUS), which has been used to estimate the detector effects on model data. HORUS is a detector simulation tool for modelling the relevant physical and electronic processes impacting the detective quantum efficiency of the Adaptive Gain Integrating Pixel Detector (AGIPD) [33] [34], which is one of the European XFEL detectors considered appropriate for the SPB instrument.

HORUS is a collection of routines aimed at the systematic study of the impact of certain detector design choices. The program is written using a modular structure, following step by step the various physical and electrical processes involved in the photon detection and signal generation process, as shown in Figure 6.
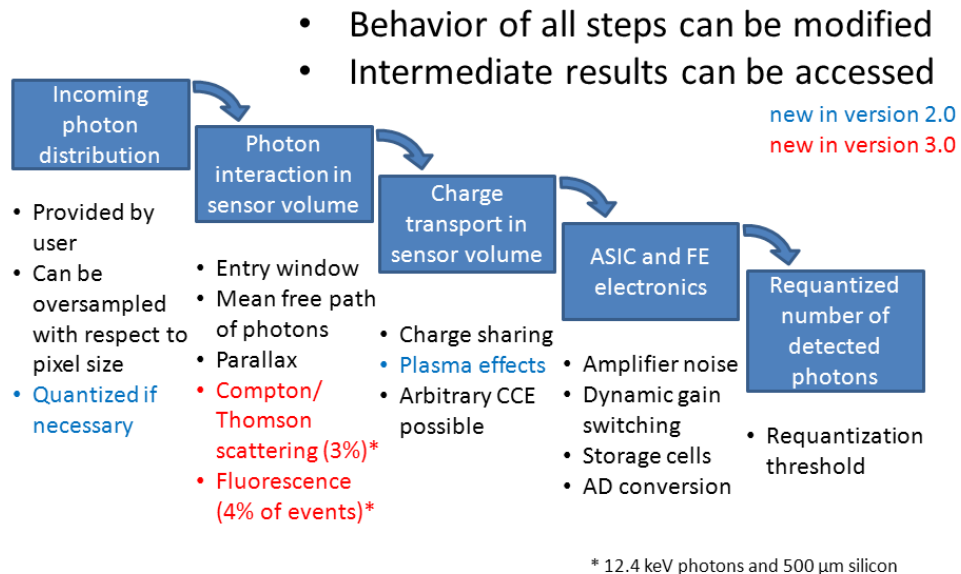
Figure 6. *HORUS detector simulation processing chain. Image courtesy of Julian Becker, DESY, Hamburg.*

The implemented models to describe the physical processes were purposely kept simple, but can be refined in future versions, if necessary. The underlying default simulation parameters are constantly updated as more data becomes available from the evaluation of the AGIPD test chips.

The detector simulation tool is part of the AGIPD project for the European XFEL and thus reflects the implementation of this detector. HORUS can be used both to study the overall detector performance as a function of various technological choices, and to simulate the degradation of any input image in order to study its impact on the scientific application.

Source photon field simulations

The source field simulation team has delivered time-dependent simulations of the source photon fields for different bunch charge operation modes of the accelerator. This data will be used as the initial input to the modelling program, when the links between the modules are established. As interim inputs, Gaussian beams of comparable size and divergence to these

simulations are used. Already, data for 0.1, 0.25, and 0.5 nC bunch charge are available with photon energies of 8 and 12 keV.

Scientific computing and image reconstruction

The data format envisaged for storing, exchanging, and recording the history of scientific data samples will be based on Hierarchical Data Format 5 (HDF5) [32]. HDF5 is capable of describing complex data objects and associated metadata in a platform-independent format. Data representation is self-describing in the sense that the format defines all the information necessary to read and reconstruct original objects of an abstract data model. The software libraries are available on a broad range of computational platforms and programming languages, which makes the data analysis highly portable. A collection of generic tools exists for managing, manipulating, viewing, and analysing data. HDF5 has recently become the standard format for handling data in many scientific disciplines, at other photon light sources, and in particular at LCLS. The high-level interface definition and its implementation optimizing access to large datasets, hiding the complexity of various data management aspects, and maintaining portability will be provided by the Data Acquisition, Data Management, and Scientific Computing teams within the European XFEL software framework.

This software framework is envisaged to also assist in processing and visualizing the image data. Predefined modules will be available that have to be extended only by the specific data processing routines. Common challenges like data input/output, handling configuration settings, error treatment, logging, multi-threading, etc. will already be solved within the pre-defined part of the modules. The modules may then be chained to form higher-level data-analysis pipelines of arbitrary complexity. New modules will automatically be available (plug-and-play mechanism) within the provided graphical user interface (GUI) for individual configuration and running, and also be available as building blocks of a user-defined analysis pipeline. The Data Acquisition, Data Management, and Scientific Computing group plans to also provide highly optimized standard image processing routines (rotations, filters, FFT, etc.) making use of e.g. GPU technology as part of the European XFEL software framework. These tools will be used in the final stage of the modelling program, to reconstruct images form the modelled data, and to

evaluate the fidelity of these reconstructions as a function of the instrument's optical layout, sample type, detector parameters, etc.

5 Optical layout

This section describes the goals of the SPB optical layout, provides an overview of the SPB instrument, and explains the choice of focusing technology. It also describes options that go beyond baseline optics as well as additional optical elements.

Goals of the SPB optical layout

The optical layout of the SPB instrument must respect the requirements presented by the three key categories of experiments outlined earlier in this document.

Specifically, across the operating photon energy range of the instrument, the optical design should ensure that:

- Maximum number of photons is delivered to the sample in a spot size comparable to the sample size.

- Minimally perturbed wavefront in the focal plane is delivered.

The SPB instrument will pursue two different-sized focal spots to match samples of different sizes, as outlined in the SPB Workshop summary document [1]. One will be a focal spot slightly larger than 1 μm, which can accommodate samples as a large as the hutch geometry and pixel size of the detector (see Appendix A, "Limitations on maximum sample size", on page 81) will allow. The other will be a sub-100 nm spot size to accommodate the smallest samples on the order of tens of nanometers.

These goals need to be achieved within the constraints of the beam size and divergence of the FEL beam, both determined by the source itself and the optical elements encountered during propagation. A summary of the expected beam sizes and divergences for the SPB instrument, as a function of photon energy, are given in Table 5.

Table 5. *Beam size and divergence at the experiment hall as a function of photon energy [23]. The upper and lower values of divergence refer to cases of differing bunch charge in the accelerator.*

Photon energy [keV]	FWHM$_{upper}$ [mm]	FWHM$_{lower}$ [mm]	Divergence [µrad]*
3	5.57	3.10	6.18
5	3.80	2.01	4.22
8	2.67	1.34	2.96
10	2.26	1.11	2.51
12	1.97	0.95	2.19
15	1.66	0.79	1.85

* Divergences are calculated for the lowest bunch charge

As can be seen, the beam in the most extreme case is very large in the experiment hall, especially for the lower photon energies, and is still large even in the expected lower bound. This is mainly due to the large propagation distance between the undulator and the experiment hall. It is this beam size, coupled with the science requirements stated above, that provide the boundary conditions for the optical design described in the following section.

Outline of the SPB instrument

The SPB instrument aims to use Kirkpatrick-Baez (KB) mirrors to deliver a spot slightly larger than 1 µm as well as a sub-100 nm spot to a common focal plane or "interaction region". At this point, the sample is injected (or in some cases mounted), the details of which are described in Chapter 6, "Sample environment and delivery", on page 48. Further downstream of the interaction region, a 2D detector is required to be located at distances from as close as possible to the interaction region through to at least 10 m downstream of the interaction region. This large variation is required to allow both the measurement of scattering signals from the smallest expected samples to angles commensurate with near atomic resolution, and to allow for appropriate sampling of diffraction patterns from samples as large as

about a micron for a coherent imaging-type inversion across the operating energy range of the instrument (see Appendix A, "Limitations on maximum sample size" on page 81). Following the detector is a so-called "intelligent" beamstop to measure shot-to-shot beam properties, and is described in more detail in Chapter 7, "Instrument diagnostics systems" on page 55. Upstream of the mirrors are further diagnostics and beam conditioning elements, such as slits prior to each optical element, to protect the optics in case they are overfilled with the beam, and attenuators to allow non-destructive beamline alignment to be performed.

To deliver the focal sizes required, we can initially consider the source size and the geometrical optics that lead to the ideal, focal-plane spot sizes. The SPB interaction region will be approximately 930 m downstream of the photon source point. This source has a size of around 40 µm for a variety of plausible accelerator parameters (see Chapter 4, "Photon beam properties", on page 17). To achieve a spot size slightly larger than 1 µm, an ideal focusing element would need to be placed approximately 24 m upstream of the interaction region. This is shown in Figure 8 as the SPB KB optics hutch. Similarly, for a sub-100 nm spot size, the focusing element is required to be about 2.4 m upstream of the interaction region. The optical design shown in Figure 7 reflects these constraints.
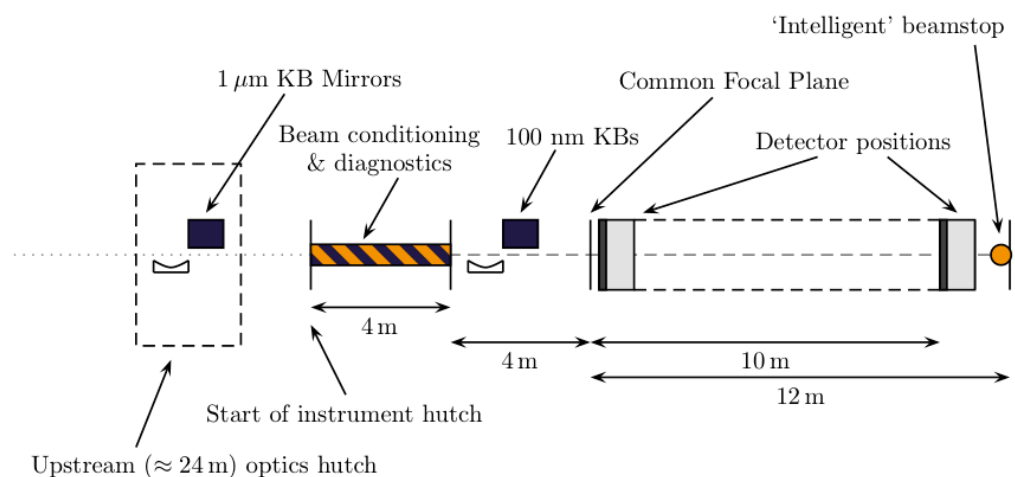
Figure 7. *Conceptual design of the optical layout of the SPB instrument. Note well the upstream optics hutch, which is to be located as far upstream as possible on the experiment hall floor. This long distance is necessary to deliver the ~ 1 µm spot requested by the single particle imaging community. Figure 8 details this approximately to scale.*
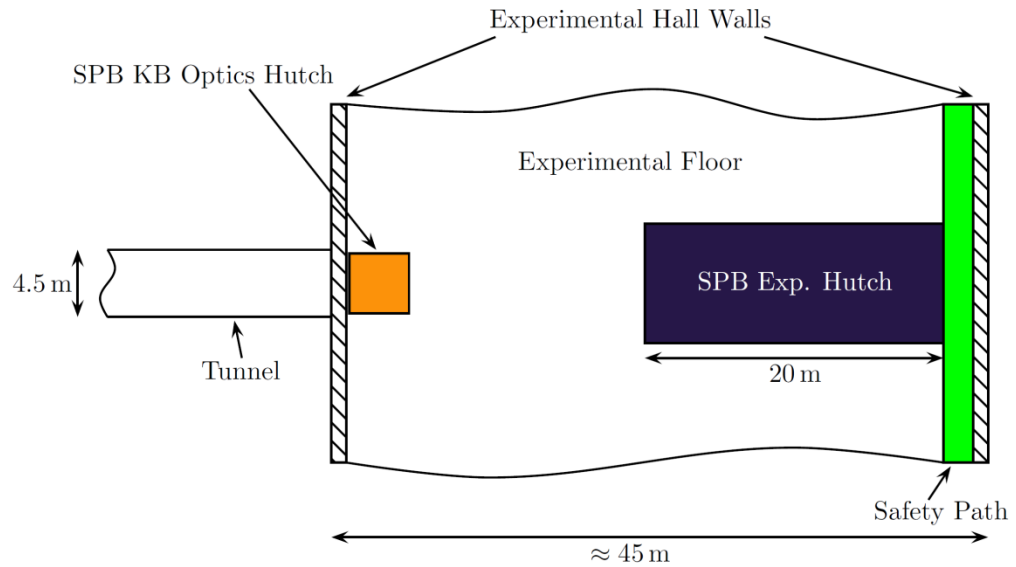
Figure 8. *Approximate scale sketch of the location of the SPB optics hutch with respect to the SPB experiment hutch and the experiment floor. The beam propagates from left to right. The KB optics hutch is located approximately 24 m upstream of the interaction region, i.e., as far upstream as possible while still on the experiment floor. The experiment floor continues in both directions perpendicular to the beam propagation.*

Choice of focusing technology

Mirror technology has been chosen for the primary optical elements for a variety of reasons that satisfy the requirements outlined above.

Mirrors are:

- Efficient, reflecting the vast majority of radiation incident on them, provided that grazing angles are below the critical angle of reflection

- Damage-resistant (for managed flux densities)

- Wavefront preserving (if length and figure error specifications are achieved)

- Achromatic, making for simple (and hence faster) alignment of the instrument

One critical condition of successfully using mirrors as X-ray optics is to ensure the mirrors are long enough to reflect a large fraction of the incident beam. This ensures good transmission of flux, essential for experiments requiring the maximum number of photons per pulse, but also avoids the introduction of structure in the beam from diffraction effects that occur when the entrance pupil of the mirror is overfilled by the X-ray beam. Table 6 shows the required lengths of mirrors, coated with different materials to reflect 4σ (of the incident intensity) of the European XFEL beam in the experiment hall, as a function of X-ray photon energy.

Table 6. Minimum mirror length for a vertical KB mirror that collects 4σ of the beam in the experiment hall as a function of mirror coating. Table taken from [23].

	3 keV	8 keV	12 keV	18 keV
C coating	1 087 mm	1 260 mm	1 339 mm	1 485 mm
Pd coating	652 mm	756 mm	803 mm	891 mm
Pt coating	481 mm	558 mm	593 mm	658 mm

We see that, for Carbon-coated mirrors, which are arguably more damage-resistant than metal-coated mirrors, the mirror lengths required are longer than present manufacturing capabilities. The European XFEL X-Ray Optics and Beam Transport team aims to make use of high-quality X-ray mirrors of 800 mm length for the offset mirrors required for safety [23]. This still requires improvements in mirror manufacture to meet length and figure error requirements simultaneously [23]. In line with the X-Ray Optics and Beam Transport CDR [23], this report considers the longest feasible length of mirror to be 800 mm.

Metal-coated mirrors, however, offer the possibility of using steeper graze angles to reflect the incident radiation, meaning that, for a mirror of fixed length, the aperture improves with respect to carbon-coated mirrors. We see in Table 6 that Palladium- or Platinum-coated mirrors can each satisfy the requirement of collecting 4σ of the delivered beam. Having established that metal-coated mirrors can accept and deliver the beam, we now consider if such mirrors will survive the FEL beam.
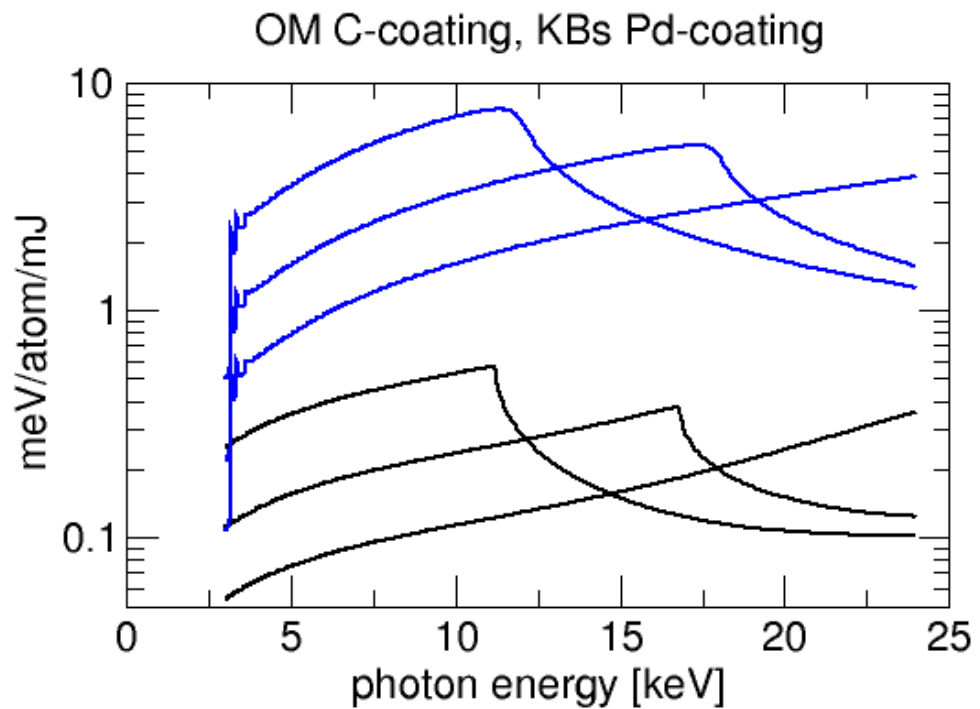
Figure 9. *Deposited energy per atom for the offset and the KB mirrors for increasingly steep graze angles. The black lines are for the offset mirrors (Carbon coated), the blue lines for the Pd-coated KB mirrors. Figure taken from [23].*

Figure 9 shows the calculated deposited energy per atom for Palladium-coated KB mirrors at angles between 2.3 and 5 mrad. In all cases, the deposited energy per atom is less than 10 meV/atom/mJ in simulations that neglect the cooling effect of photoelectron transport. Assuming that damage occurs for a deposited energy of about 0.5 eV/atom for Palladium, an almost two-order-of-magnitude safety margin would be observed here if a Palladium coating was used on the SPB mirrors. A possibility to further protect metal coatings from the FEL beam is to deposit a Silicon Carbide coating over the metal coating [35], which also has the advantage of improving the reflectivity of the mirrors across a wide range of photon energies. The limitation in both cases described here is given by the small amount of experimental data about damage to these kinds of coatings in an FEL beam and the limitations of the models used presently to estimate the damage in the coatings and substrates. This key question of damage will be investigated more closely in the technical design phase. Furthermore, despite their resistance to single shot damage, these mirrors will require cooling to prevent melting during the full pulse train.

Optical layout of the SPB instrument

The SPB optical layout is sketched above in Figure 7. Essentially, the key focusing optics are two KB mirror pairs that focus to a common plane within a vacuum sample environment. The mirror pairs will each be controlled such that they can be driven out of the optical path of the FEL beam to allow either pair to be used at a given time. The upstream mirror pair aims to produce a spot slightly larger than 1 μm from metal-coated mirrors of 800 mm length, which can capture more than 4σ of the beam for photon energies between 3 keV and 12 keV. The downstream pair aims to produce a sub-100 nm focus from shorter mirrors of about 550 mm in active length, or longer if determined to be technically feasible. These will also be coated with metal to improve the aperture of the optics, although it will capture commensurately less of the FEL beam unless it is prefocused.

The sub-100 nm KB pair can be designed to accept a converging beam from the 1 μm optics in order to optimize the total photon flux delivered to the sample from a single shot. Later modelling will determine if this prefocused geometry is feasible. If so, the 1 μm KB pair will need to be bendable, to alter the focal point allowing the 100 nm mirrors to focus to the common focal plane. Both the feasibility of 800 mm bendable mirrors and the damage thresholds of the coating under the increased prefocused flux will need to be assured before pursuing this model. In the absence of prefocusing to the 100 nm mirrors, the focal point produced by the two different mirror systems will be quite some transverse distance apart—up to some few hundred millimetres, depending on the mirror angles—requiring precision motion control over this distance to align the instrument for each case. Both this option of directly focusing to a 100 nm spot and that of prefocusing before the 100 nm optics will be pursued in the technical design of the SPB instrument to mitigate the difficulties associated with each course of action.

Ideally, the SPB instrument will be equipped with two detectors, one of which will be located very close to the interaction region on a rail allowing about 1 m travel in the direction of the beam and the other much further downstream on a rail allowing travel between about 6 and 10 m downstream of the interaction region. This detector arrangement allows for the well-sampled collection of the necessary-for-reconstruction low-frequency information in the diffraction data on the downstream detector, while high-resolution information at a high

angle is simultaneously collected in the upstream detector (see, for example, Appendix A, "Limitations on maximum sample size", on page 81). A two-detector arrangement also mitigates the need for an ultrahigh dynamic range, by splitting the required range across two devices (see Chapter 9, "Detector system", on page 65). Initially, a single detector for the SPB instrument is included in the overall European XFEL detector plan.

Simulations of the 1 µm focal spot

Some initial simulations of the 1 µm spot have been performed by Liubov Samoylova of the European XFEL and collaborators using the SRWLib code package [28]. The initial simulations shown here make some simplifying approximations, which will ultimately be replaced by more realistic models during the technical design phase. We consider two photon energies, 12 keV and 5 keV. The effects of the horizontal offset mirrors (HOMs) in the X-ray beam transport [23] are modelled with realistic figure errors, similar to those measured for mirrors used at LCLS. We model the KB optics by a thin lens, an aperture with a size governed by the mirror length and the incident angle and add realistic height errors (similar to the HOMs) as an aberration to this lens, governed by the incident angle of the beam. These simulations consider the optic-to-sample distance to be 35 m, though this distance has since been revised. Following the suggestion of the ART, we now consider the optic-to-sample distance to be 24 m—ensuring the optics are on the same concrete slab as the end station for vibrational reasons—and the modelling of 24 m optics performance is presently in progress.

Table 7. Graze angle as a function of mirror coating and photon energy as used for the simulations of the SPB instruments 1 µm focal spot. The angles here were used to determine the size of the aperture of the mirrors.

| Photon energy	Graze angle (C) [mrad]	Graze angle (Pd) [mrad]
5 keV	5	7
12 keV	1.8	3.6

The source is presently modelled as an ideal Gaussian beam with far-field divergence as a function of photon energy taken from Schneidmiller & Yurkov's simulated values of the FEL photon beam parameters [29], in this case for a bunch charge of 100 pC. The beam is propagated to the horizontal

offset mirrors, which are 270 m from the source. The beam then reflects from the two offset mirrors. The second offset mirror is designed to have the capability of bending and hence focusing the FEL beam; however, these simulations consider the case where the second mirror is bent to be plane. The beam is then propagated in free space to the entrance of the KB mirrors and is shown for the 12 keV case below in Figure 10.
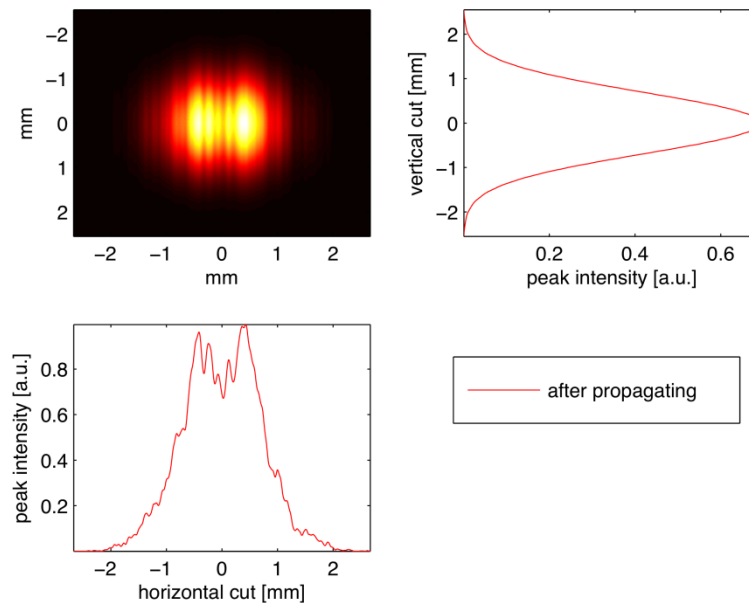
Figure 10. *Modelled 12 keV European XFEL beam in the optics hutch prior to the 1 µm KB mirrors after propagating from the source via the horizontal offset mirrors (HOMs), including realistic estimates of height error for the HOMs.*

We then consider the case where the KB mirrors are carbon-coated, 800 mm in length, and with a focal distance of 35 m. Figure 11 below shows the intensity and a profile of the phase of the beam in the focal plane. Note that, in all of the examples below, the phase is uniform or very slowly varying in the focal plane, which are excellent wavefront conditions for plane wave coherent imaging.
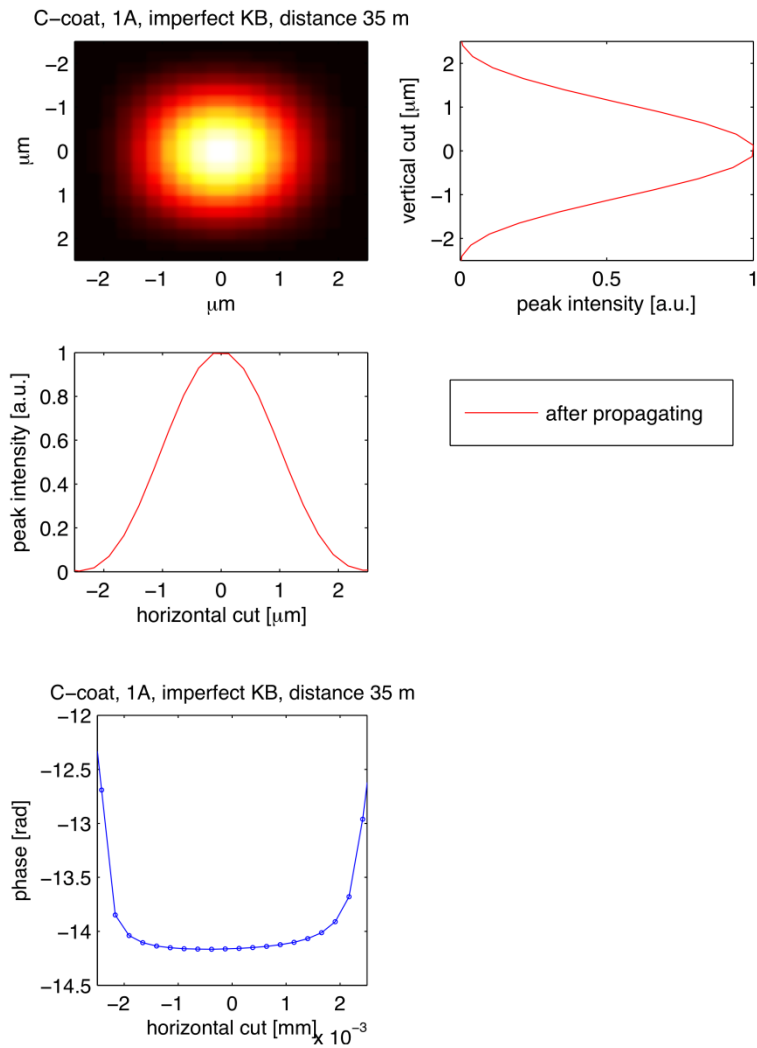
Figure 11. Intensity and phase of the 12 keV beam in the focal plane from a carbon-coated KB pair (modelled as a lens with aberrations that correspond to realistic height errors) with ~ 35 m focal length and an aperture governed by the 800 mm length mirrors. The total transmission of the system is about 41%.

We now consider the case where the KB mirrors are Palladium-coated, for the same parameters (except the graze angle, which is steeper as per Table 7).
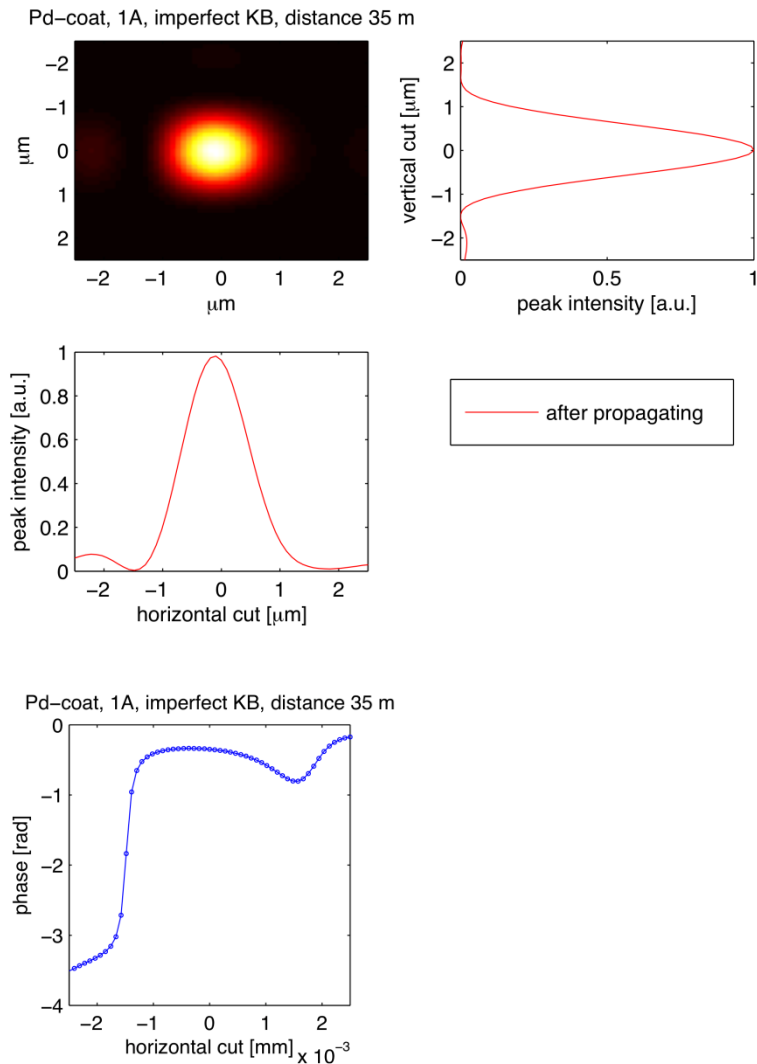
Figure 12. *Intensity and phase of the 12 keV beam in the focal plane from a Palladium-coated KB pair (modelled as a lens with aberrations that correspond to realistic height errors) with ~ 35 m focal distance and an aperture governed by the 800 mm length mirrors The total transmission of the system is about 76%.*

We see a considerable benefit in the transmission of the Palladium-coated mirrors with respect to the Carbon-coated mirrors, due to the improvement in aperture that the higher graze angle of Palladium affords. We also see in Figure 13 that an extremely long depth of focus is achieved, which is beneficial for imaging injected samples.
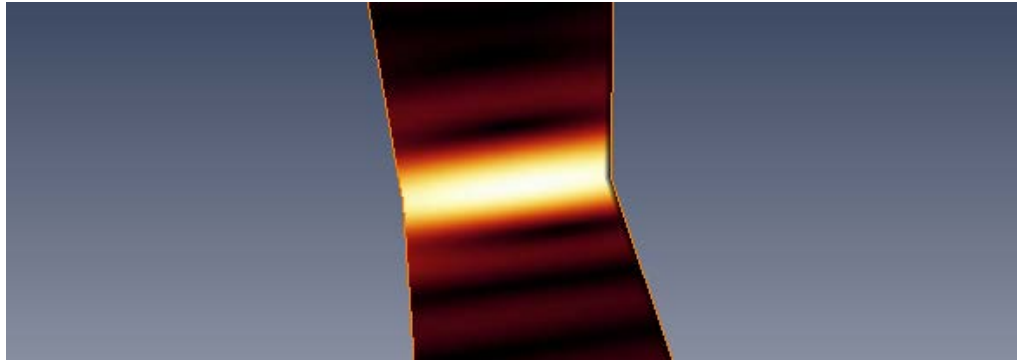
Figure 13. Longitudinal profile of the nominally 1 µm focal spot for 12 keV radiation and Pd-coated mirrors. The longitudinal dimension of the intensity profile shown is 14.5 mm. Note the extremely long depth of focus (even longer than shown here), which is of great benefit for the coherent imaging of injected samples.

Similarly, for the 5 keV case, we see the beam after the HOMs and prior to the modelled KB mirrors in Figure 14 below.

Figure 14. Modelled 5 keV European XFEL beam in the optics hutch prior to the 1 µm KB mirrors after propagating from the source via the horizontal offset mirrors (HOMs), including realistic estimates of height error for the HOMs.

We now consider the focusing produced by the same KB model with aperture limited by a carbon coating.
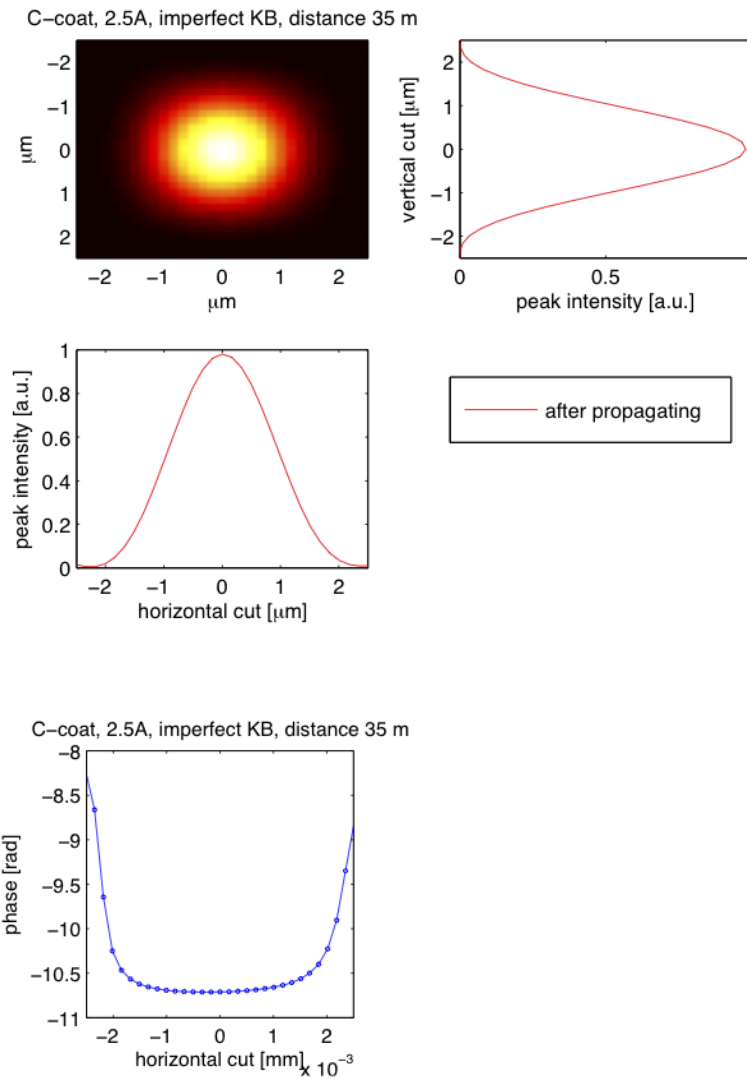
Figure 15. *Intensity and phase of the 5 keV beam in the focal plane from a carbon-coated KB pair (modelled as a lens with aberrations that correspond to realistic height errors) with ~ 35 m focal distance and an aperture governed by the 800 mm length mirrors. The total transmission of the system is about 55%.*

Figure 16 shows the result of the simulation for a Palladium coating, again showing an improved transmission of the optical system and smaller focal spot sizes. This is predominantly due to the larger aperture that Pd-coated mirrors afford the optic.
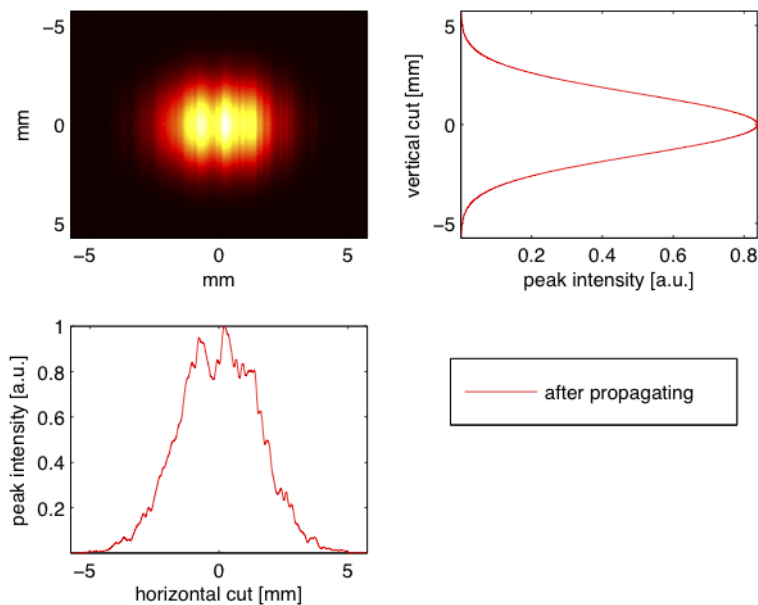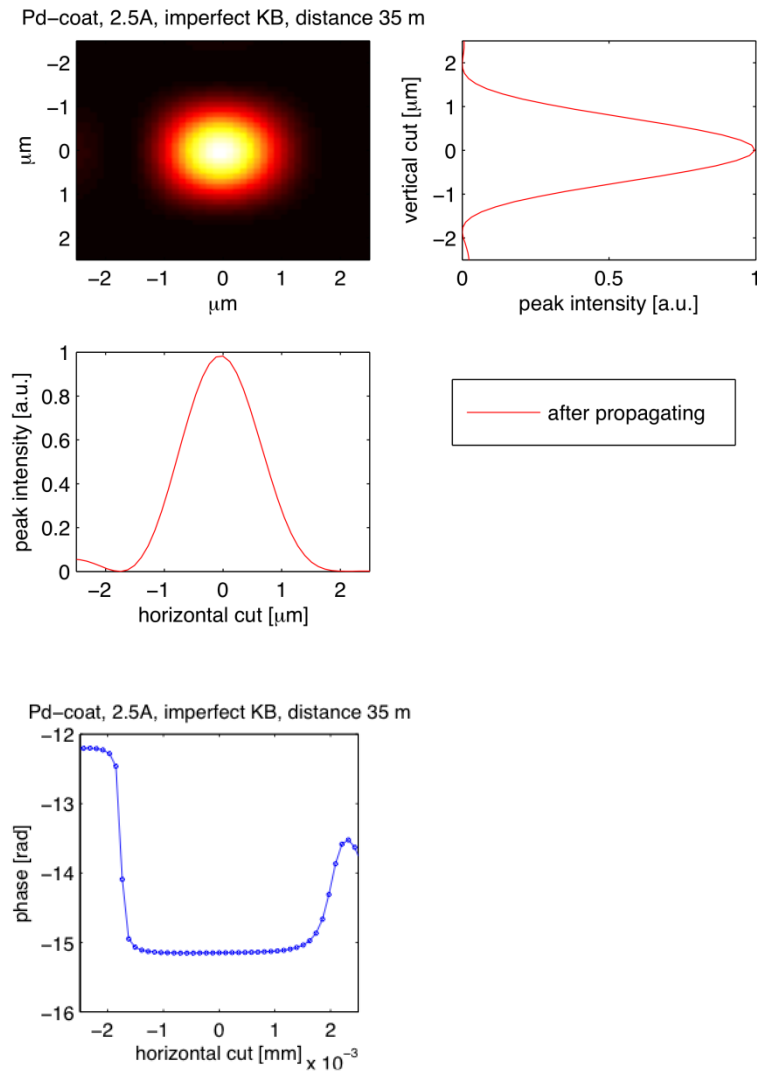
Figure 16. *Intensity and phase of the 5 keV beam in the focal plane from a Pd-coated KB pair (modelled as a lens with aberrations that correspond to height errors) with ~ 35 m focal distance and an aperture governed by the 800 mm length mirrors. The total transmission of the system is about 74%.*

Simulations of the nano-focal spot

Similar simulations have been performed for the 100 nm focus, again for 12 keV and 5 keV radiation using the same process described for the 1 µm mirrors. The difference is the mirror length, which is 600 mm here, with a useful length of 550 mm. The effective optic to interaction region is 1.4 m. Note again the very flat phase profiles indicating appropriate conditions for plane wave coherent imaging.
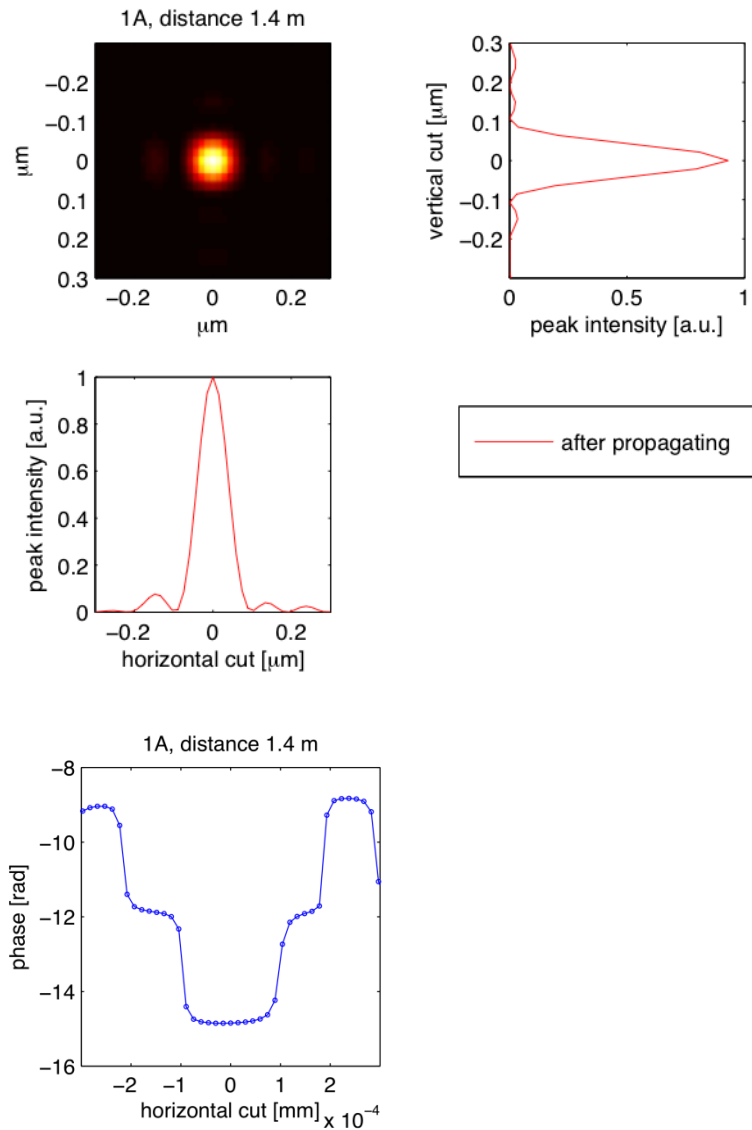
Figure 17. *Intensity and phase of the 12 keV beam in the focal plane from a Palladium-coated KB pair (modelled as a lens with aberrations that correspond to realistic height errors) with 1.4 m focal distance and an aperture governed by the 550 mm usable length mirrors. The total transmission of the system is about 48%.*

Figure 18. Longitudinal profile of the nominally 100 nm focal spot for 12 keV radiation and Pd-coated mirrors. The longitudinal dimension is 1 mm. Note again the long depth of focus.
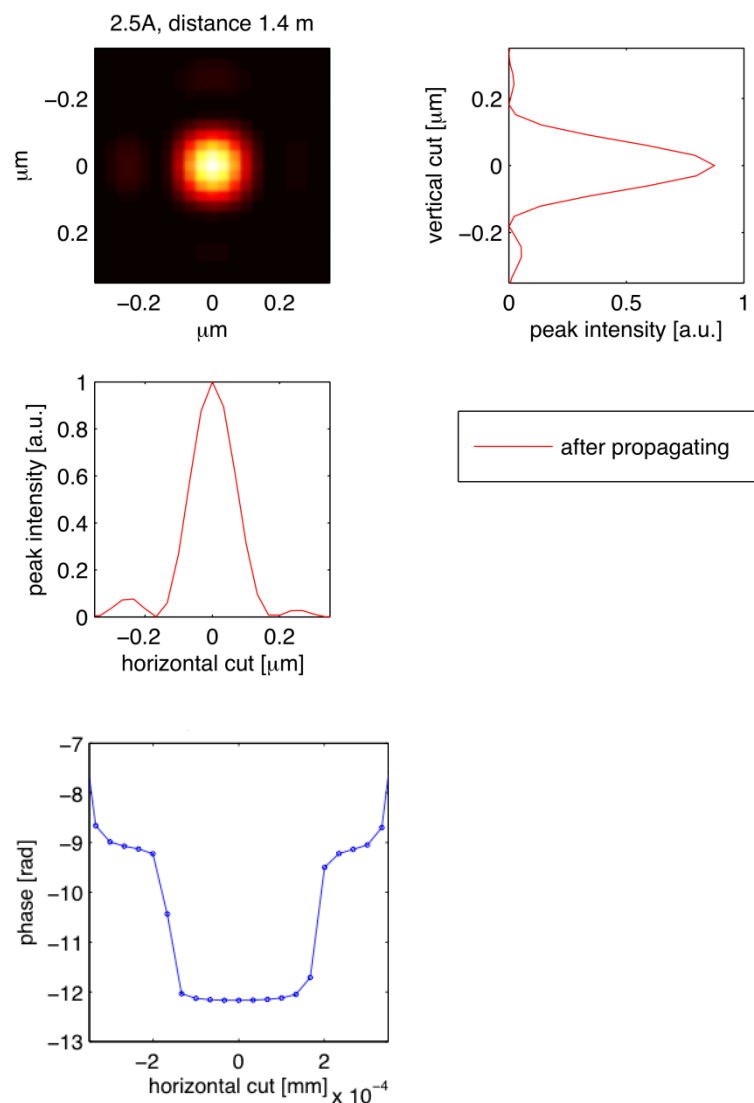
Figure 19. Intensity and phase of the 5 keV beam in the focal plane from a Palladium-coated KB pair (modelled as a lens with aberrations that correspond to realistic height errors) with 1.4 m focal distance and an aperture governed by the 550 mm usable length mirrors. The total transmission of the system is about 22%.
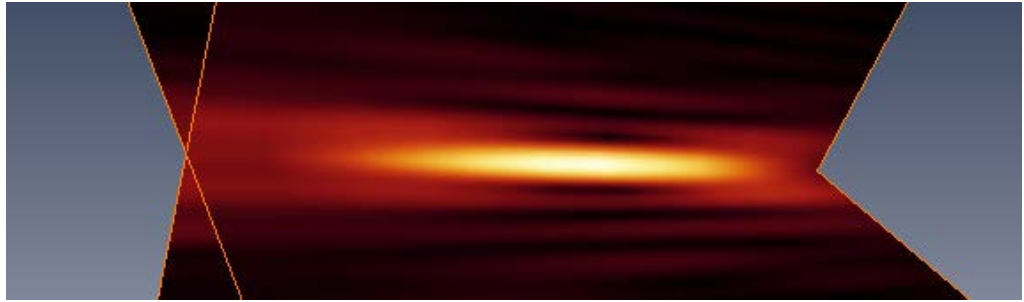
The lower transmission of the 5 keV radiation is primarily due to the larger beam size in the experiment hall at these energies, though is still quite high for a nanofocusing optic. For a 250 pC bunch charge with the accelerator operating at 14 GeV electron energy, one expects to produce about 1.3×10^{12} photons/pulse at 5 keV [29]. Assuming no further losses than those considered here and leading to Figure 19, this amounts to about 2.6×10^{11} photons/pulse in a 100 nm focal spot.
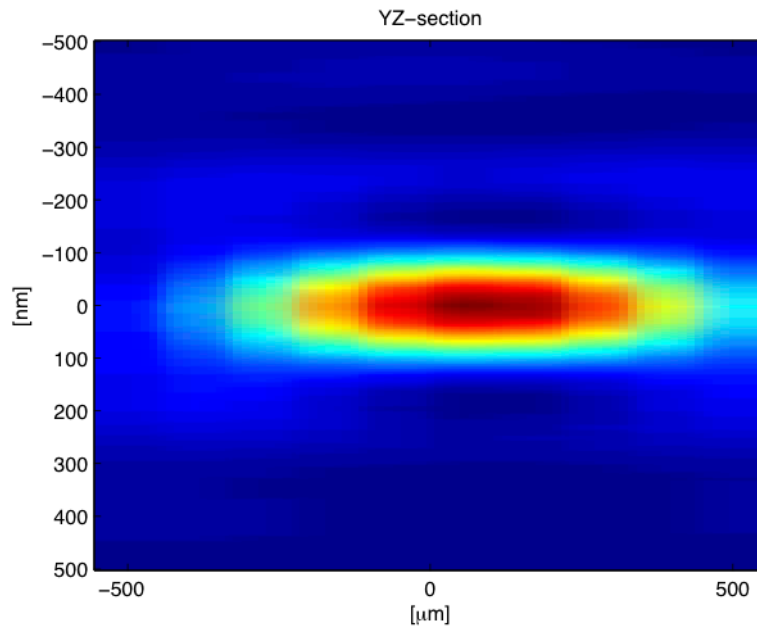
Figure 20. *Sections of the 5 keV, 100 nm beam focus shown perpendicular to the direction of propagation. Note again the large depth of focus, here a few hundreds of microns.*

While the large source to focusing optics distances make capturing a large fraction of that divergent beam challenging, this same quantity also means that the optics deliver very large focal depths, with flat wavefronts, over distances much larger than the diameter of injected sample streams. This not only eases sample-beam alignment, but also allows for the use of larger sample streams to increase hit rates while keeping the injected sample in the focus of the beam.

Conclusions

We see from the simulations that the Pd-coated mirrors perform considerably better than their carbon coated counterparts in terms of spot-size and total transmission, due primarily to the larger aperture afforded by working at steeper angles. Note that for steeper angles (Pd-coated mirrors) the height errors impact the performance of the optic and the spot size broadens with respect to a "perfect" mirror. This is more noticeable at 12 keV, where the corresponding wavefront errors are proportionally larger, and less of a problem at 5 keV. We note, however, that the Pd-coated mirrors still produce a smaller focal spot than the carbon-coated mirrors, in both cases explored above. Given the generous gap between the calculated energy deposited in these mirrors per pulse, and the estimated damage threshold of Pd, we conclude that metal-coated mirrors are an appropriate solution for the focusing needs of the SPB instrument with an unfocused incident beam.

"Beyond baseline" optics options

This section describes options for optics that go beyond the baseline design.

Possible user contribution

We briefly consider an extension to the optics, which is beyond the baseline design, as proposed under the User Consortia Expressions of Interest program of the European XFEL [36]. The particular proposal is known as "Serial Femtosecond Crystallography" (SFX) and is proposed by a consortium led by Henry Chapman of the Centre for Free-Electron Laser Science (CFEL) in Hamburg. The design outlined below accommodates this proposal, or any similar refocusing option, with minimal changes to the baseline SPB design. Note that the design below differs only from the baseline SPB design by the addition of the refocusing optics after the upstream detector and the increase in size of that detector to 4 Mpx.

Refocusing

The "refocusing" beyond-baseline option represents an extension from the baseline operation of the SPB instrument to include a refocusing optic behind the detector, which would be positioned in a far upstream position, and a second interaction region installed at the downstream end of the instrument. This would then accommodate the reuse of the beam for sample screening or a second experiment that can utilize the beam conditions of the beam used upstream. In particular, experiments that are less demanding on the optical properties of the beam, such as nanocrystallography, could be performed with a refocused beam.
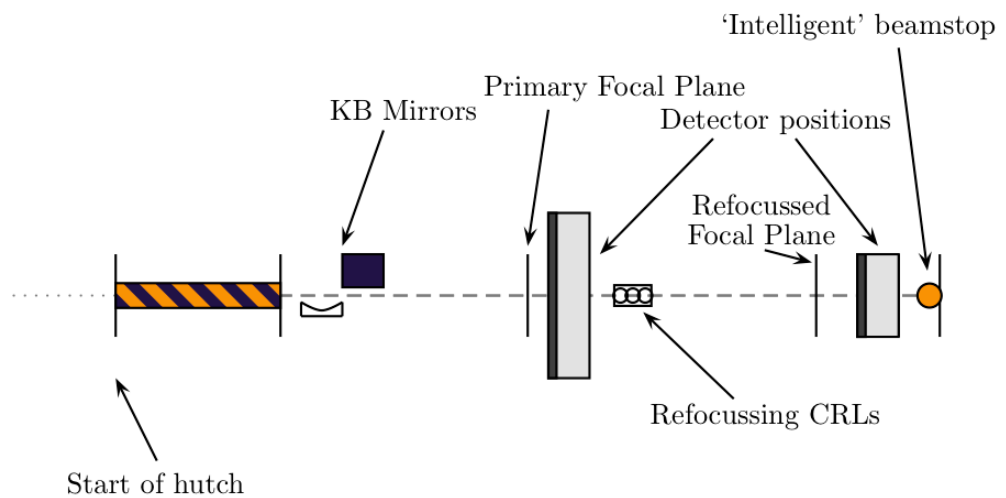
Figure 21. Refocusing option. The length of the entire instrument can benefit from being slightly longer in the refocusing case, in order to fit the additional optics and interaction region in the instrument hutch.

Choice of focusing technology: compound refractive lenses

CRLs as refocusing optics have the key advantage of a short longitudinal profile and an on-axis operation. As the experiments that would take place in the refocused beam would likely have a less stringent requirement on the beam's wavefront (for example, sample screening or nanocrystallography), the graininess of the materials used for CRLs is less of a problem. They can also be readily inserted or removed to minimize disruption to the main experiment should measurements downstream be needed.

Alternative choice of focusing technology: KB mirrors

A small KB mirror pair could be an alternative refocusing option to the CRLs described above. The challenges here are ensuring that such a mirror survives the power density incident upon it, which is larger than for the other optical elements in the beamline and the end station. The benefit is achromatic operation, but the cost is the loss of in-line operation of the instrument downstream of the refocusing element. The broader ramifications of this option will be examined in the technical design of the SPB instrument.

Other optical elements

Other optical elements include apertures, attenuators, and a monochromator.

Apertures

The apertures used in the SPB instrument will be those described in the X-Ray Optics and Beam Transport CDR [23], which are composed of Boron Carbide and Tungsten and have been designed specifically for the high repetition rate of the European XFEL. In particular these apertures will be water-cooled and can operate in the full pulse train of the European XFEL across the operating photon energies of the SPB instrument.

Attenuators

The most important property of the attenuator, apart from attenuating the beam, is to also minimize the disturbance to the beam's wavefront as it traverses the attenuation material. This means the attenuators should be manufactured from a homogenous material, of uniform thickness, that can attenuate the European XFEL beam without being destroyed by that same beam. A candidate material may be single-crystalline, water-cooled diamond in a variety of thicknesses leading to discrete attenuations of a few steps per order of magnitude across the instrument's operating range.

Monochromator

A monochromator is not an essential element for the success of the SPB instrument (see for example [22]) and is considered an optional, later-stage addition. It is, however, advantageous for experiments benefitting from a

higher longitudinal coherence length, or the precision to work precisely at elemental absorption edges. The key requirements are a best possible conservation of X-ray wavefronts and the stability of the beam position. The concept of a silicon-based, artificial channel-cut should be appropriate, as it allows independent polishing of the reflecting surfaces to the highest quality levels. Because the two crystals are then mounted onto the same rigid support, the monochromator is rather insensitive to vibrations.

Heat load calculations show that up to 1 000 pulses per pulse train could be transmitted for 250 pC operation, if the first crystal is cooled cryogenically [23] and the monochromator is positioned in the unfocused beam at the end of the photon tunnel.

In the conceptual design report of the X-Ray Optics and Beam Transport group [23], such a design is proposed and a prototype will be built and tested.

6 Sample environment and delivery

This chapter describes the general sample environment, sample injection technology, and fixed sample-mounting system, as well as additional sample injection technology, for the SPB instrument.

General sample environment

The SPB instrument will be an in-vacuum instrument, including at the sample environment. This is mainly to reduce the unwanted effects of air-scatter in the experiment, namely absorption and background. The feasibility of alternative environments, such as a helium environment, will be investigated in the technical design of the instrument.

The sample environment is envisaged to comprise a single chamber surrounding the common focal plane of both the 1 µm and 100 nm optics, assuming this is technically feasible. The primary method of introducing samples to the interaction region will be by injection. In addition, fixed samples will also be accommodated.

The presence of fluids in the vacuum chamber will require the careful use of differential pumping and an efficient trap or sample collection system to protect both the optics and the detector systems. Precision motion control of the sample injection systems will also be necessary to deliver the sample to the micron and sub-micron scale interaction region.

Sample injection technology

In order to observe biological structure in a state most resembling the native state, it is necessary to have the capability to work with hydrated, non-frozen biological samples. Two types of sample injectors presently in use at X-ray sources are liquid jets and gas phase streams. Both are able to produce highly collimated, high-number density, continuously flowing, hydrated sample streams. Both produce sample streams without confining walls or supports—no part of the injector reaches into the X-ray interaction region; as a result, the injector itself does not contribute to the background signal. Pulsed sample sources are presently under development.

Liquid jets

It is often possible to inject the sample into the X-ray beam in the same solution in which it was grown or purified. Using a very thin, rapidly moving column of liquid, called a jet, the sample solution can be positioned very accurately within the X-ray interaction region. Diffraction patterns obtained using a liquid jet have a substantial contribution from the liquid surrounding the object of interest and from the shape of the jet itself. To minimize this water background, jet size should be matched to sample size. The current state of the art is about 500 nm in diameter for water jets and as small as 300 nm for jets of lower surface tension [37]. Research is under way to produce smaller jets with the near term goal of 100 nm for water. Models for liquid water jets show no lower limit to jet size [38].

Micron-sized liquid jets are produced by a nozzle with a large, 20–50 micron diameter, exit aperture surrounded by a coaxially flowing gas [39]. There are no solid constrictions in the lines carrying the sample—the jet diameter is reduced through gas dynamic forces. As the liquid is accelerated through the pressure gradient of the surrounding gas, it becomes thinner. This has two main advantages over converging channel nozzles: a) reduced incidence of clogging and b) reduced flow rate. The first advantage is clear: without a solid converging channel, there is little possibility of particles getting stuck in the nozzle. Particles much larger than the jet diameter can pass through the nozzle exit. The reduced liquid flow rate, roughly 1 microliter/minute for 1 micron diameter, is due to the stabilizing effects of the gas on the liquid

surface [40]. In the absence of an accelerating gas, Rayleigh jets move at much higher average fluid speed resulting in an order of magnitude higher flow rate for a similar size jet. The advantage of a reduced flow rate is less waste of precious sample material.

The high repetition rate of the European XFEL, combined with the high hit rate and rapid sample replacement obtained with a liquid jet, will permit full micro- or nano-crystal data sets to be obtained in minutes to tens of minutes with minimal sample consumption. Liquid jets are very well suited to both the expected 1 μm X-ray focus at the SPB station and the X-ray repetition rate. To maximize the efficiency with which the sample is used, the speed of the jet should be such that the sample moves through the interaction region no faster than necessary. For example, for a 1 μm focus and X-ray pulses separated by 220 ns, the jet must move at (1 μm / 220 ns =) 4.5 ms^{-1} in order to supply sample to the interaction region fast enough to utilize all pulses. Fortuitously, this is the approximate speed of a 1 μm jet. It is likely that radiation damage will extend beyond the 1 μm focus and the jet will need to move somewhat faster, but increasing the speed of a liquid jet can easily be accommodated. In microcrystal experiments that have been carried out at the LCLS, the probability that each X-ray pulse will intercept a crystal has been between 1% and 10% using a 10 μm^2 X-ray focus. Using a 1 μm focus, we would expect a factor of 10 lower hit rate, which implies a collection rate of 30 to 300 diffraction patterns per second or 10^5 to 10^6 patterns per hour. For a flow rate of 60 μl/min, this would consume only 60 μliter of sample at a concentration of 10^9 crystals/ml—a reduction by a factor of 100 from what is currently required.

Advantages:

- Very accurate positioning of the sample solution

- Fully hydrated

- Many compatible solutions (sucrose, ammonium acetate, PEG, sea water, etc.)

- Sample completely replaced between X-ray pulses

- Flow-alignment of certain samples

Disadvantages:

- X-ray scattering from the water

- X-ray scattering from the jet edges

- Degree of hydration is not variable

Aerosol streams

Aerosol flows are an excellent option for smaller samples that can tolerate or require a lesser degree of hydration. For samples that are tens of nanometres in diameter, liquid jets of hundreds of nanometres in diameter are an unsuitable method of delivering the sample to the interaction region, as the background from the liquid will be many orders more intense than the signal from a small sample contained therein. An aerosol jet produced by an aerodynamic lens [41] [42] can produce a highly collimated particle stream with a variable degree of hydration.

Aerosols have particle density that is too low to obtain a reasonable hit rate unless in a focused gas flow. An aerodynamic lens consists of a series of small focusing apertures through which a particle-laden gas flows. As the gas moves through each aperture, the particles' inertia causes them to slip slightly across the gas streamlines towards the centre line. The lens must be properly tuned in aperture size and spacing to the particle size, gas speed, and density for the right balance of inertial and viscous forces [43]. As the gas flows through the entrance stages of the lens, water can be removed by evaporation; however, the removal of water from hydrophilic samples requires further investigation. Some care must aslo be taken in sample preparation as all nonvolatiles will condense on the sample.

Hit rate, the number of diffraction patterns recorded per unit time, is similar to that obtained in liquid jet microcrystal experiments. Recent experiments at LCLS obtained hit rates from a few tenths of a percent using a 1 µm X-ray focus and 30 µm diameter sample stream, to an almost 50% peak hit rate and 10% average hit rate with a 3–5 µm focus. This would correspond to at least 100 hits per second at the European XFEL using a similar-size focus and, as with liquid jets, entire data sets may be obtained in tens of minutes. 10^5 frames would be collected in less than 20 min, possibly much less. Proper alignment of the sample beam can be difficult at low hit rates. This is

sometimes a problem for low pulse repetition rates, such as at existing X-ray FEL sources; however, this problem is expected to be solved with the planned high repetition rate at the European XFEL.

As with jets, the sample moves sufficiently fast, in this case 50 ms^{-1}, to replace the sample during the interval between pulses. Because the aerosol stream and liquid jet move at roughly the same speed, but the aerosol stream is much larger in diameter, it consumes more sample—two orders of magnitude more sample. This makes it more suitable for high number density samples such as cells, viruses, and single molecules.

Advantages:

- Variable degree of hydration

- Less water background than with jets

- Sample completely replaced between X-ray pulses

- Easier sorting of diffraction patterns and removal of frames without diffraction data

Disadvantages:

- Potentially higher sample consumption

- May not be suitable for samples that require a high degree of hydration

- Evaporation will change the concentration of non-volatiles

Fixed sample-mounting system

There exist classes of samples that are either not amenable to being injected, have a preferred orientation to be presented to the beam, or exist only in small quantities. These classes of samples are best mounted in a fixed, cooled mounting system in the sample chamber where their preferred orientation may be presented to the FEL beam or where each specimen is guaranteed to be hit by a single pulse of FEL radiation. An example of this may include the Nuclear Pore Complex [15], which is a relatively flat biological structure that is difficult to purify and prepare in large quantities. A further example may be 2D crystallography [44], where injection is not

appropriate (the samples are fragile) and knowledge of the orientation is beneficial to understanding the structure.

The fixed-mounting system will have the capacity to include many small samples within the sample chamber simultaneously, to minimize the downtime associated with changing sample. The combination of many samples (which implies a large travel range) and small X-ray beams (less than 100 nm) places stringent requirements on the sample stages used to position the fixed samples in the beam. Suggested parameters would be in-vacuum stages that can travel up to 50 mm both horizontally and vertically, with reproducibility of position better than 10 nm. Stages meeting these requirements are today commercially available (see, for example, www.smaract.de).

Cryo-cooling capability (option)

The sample stage will have the capability of being cryo-cooled, using an adaptation of a commercial cryo-cooling device, either in a short region out of vacuum with a Cryostreamer [45] or in-vacuum with a cryo-system similar to that used in electron microscopy (see, for example, www.fei.com/products/transmission-electron-microscopes/titan/krios.aspx). Special care will be taken in designing the sample environment to minimize ice contamination [46].

Sample delivery diagnostics

An important aspect of sample delivery is knowing when that sample has been successfully delivered. The SPB instrument envisages incorporating a fluorescence detector and an electron Time of Flight (eTOF) spectrometer for hit detection and vetoing data. These detectors and the vetoing scheme are discussed in Chapter 9, "Detector system", on page 65 and Chapter 10, "Data acquisition, management, and analysis", on page 74, respectively.

Additional sample injection technology (option)

An additional sample injection technology known as Controlled Molecules (COMO) has been proposed under the User Consortium Expression of

Interest program [36] by a collaboration led by Jochen Küpper of the Centre for Free-Electron Laser Science, DESY, Hamburg. This injection technology [47] [48] would be able to deliver state-, size-, and isomer-selected samples of polar molecules and clusters. This addition would allow the preparation of "clean" samples for investigations of the quantum nature of larger and more complex molecular systems, as well as the imaging of such systems.

7 Instrument diagnostics systems

This chapter describes the diagnostic systems for the SPB instrument, including beam position monitors (BPMs), screens, single-shot flux monitor(s), a fluorescence spectrometer, a wavefront measurement device (WMD), a single-shot λ spectrometer, an "intelligent" beamstop, a coherence monitor, alignment laser(s), and a timing monitor.

Beam position monitors (BPMs)

The BPMs, as used in the beam transport region of the facility between undulator and experiment hall, fall into three classes:

- Gas-based online BPMs [49] that can accept full pulse-trains without risk of damage at the cost of limited resolution and rather bulky hardware, since they require differential pumping towards neighbouring UHV sections

- Invasive monitoring with screens or solid-state-based position monitors, such as semi-transparent diamond Position Sensitive Detectors (PSDs)

- Monitors ranging in application in between the first two categories, using backscattering from thin foils and detection in quadrature diodes

These monitors will have the advantage of allowing for online monitoring, but have application range limitations due to single-shot damage and pulse-train heat loads; also, there will be certain experiments, likely many of those at SPB, that cannot tolerate the degradation of wavefront and transverse coherence inherent to these monitors.

These monitors are essential to the efficient and accurate alignment of the beamline and instrument. Combinations of these differing solutions can be placed upstream and downstream of the focusing optics and after the final detector (as part of the "intelligent" beam stop). These elements may also perturb the beam and, as such, will need to be mounted in a manner that

allows them to be retracted from the optical axis and out of the beam. A combination of non-invasive and removable invasive BPMs will be used at the SPB instrument, with the requirement on removing devices that may perturb the beam paramount, in order to preserve the beam wavefront. This is more broadly a general requirement for the SPB instrument diagnostics.

Screens

A number of YAG screens [50] will be positioned along the beamline for diagnostic purposes, particularly upstream of the optics and slits. These screens will come in two basic varieties—beam stopping and beam transmissive—to facilitate basic alignment of the instrument. Thin (~ 15 µm) YAG screens have been shown to produce significant fluorescent light under illumination from FEL beams, while being transmissive enough to be seen on a similar downstream screen. These will be essential for instrument alignment, for example, but will be need to be retracted from the beam path for data taking.

Single-shot flux monitors

An absolutely calibrated (< 10% measurement uncertainty) measure of the photon flux with high shot-to-shot accuracy (relative accuracy 1–2%) across the instrument's energy range upstream of the SPB instrument will be provided by the Photon Diagnostics group [51] in the form of an X-ray Gas Monitor Detector (XGMD). It will be beneficial, however, to have a measure of the shot-to-shot flux at the SPB instrument both prior to the beam's interaction with the sample and downstream of the sample to optimize the beamline for a given configuration and to normalize measured data. These monitors are envisioned to be smaller, streamlined versions of those installed in the tunnel upstream of the SPB instrument. One ingredient for this simplification is to suppress the requirement for absolute calibration, as a relative monitor can be benchmarked against the upstream, absolutely calibrated device. This will simplify the monitors and drive down costs.

For parts of the instrument where space is at a premium, retractable semi-transparent, solid-state diamond flux monitors with very small footprints will also be available. These will be particularly valuable immediately upstream and downstream of focusing optics, for example, as well as at the end of the SPB instrument as part of the "intelligent" beamstop device.

An XGMD could ideally be an online, continually measuring device, for example downstream of the 1 μm mirrors. This may be possible due to the long distance (∼ 24 m) between them and the interaction region. Questions of the precise geometrical location of components will be addressed in detail in the SPB technical design.

Fluorescence spectrometer

A single-shot fluorescence spectrometer would allow the understanding of the state of ionization of a given atomic species in a sample (in particular metals), which could assist in the anomalous phasing of both nanocrystals and other single particles. One possible realisation of the fluorescence spectrometer could be a pixel array detector oriented at 90⁰ scattering angle, operating in an energy-dispersive mode.

Wavefront measurement device (WMD)

The wavefront of the FEL pulse incident on the sample can be of great importance to the imaging problem. It is not yet known whether the incident wavefront changes from shot-to-shot or varies over time. A changing wavefront means a changing "image" of the sample, should those variations be on the scale of the sample under investigation. Measuring the wavefront will allow one to account for the effect of the wavefront on the final image and to reconstruct an image predominantly independent of the structure of the incident beam. The WMD will likely be a destructive device that will form part of the "intelligent" beamstop (see '"Intelligent" beamstop' on page 59) at the most downstream location of the SPB hutch. It will most likely operate by using interference from gratings [52] or using variations of coherent imaging

techniques [53] [54]. In the best case, the WMD will need to be deployed only intermittently, but to anticipate the most difficult case the device should aim to operate in a shot-to-shot mode.

The measurement of wavefronts will most likely be performed as an experiment in itself during the beamline commissioning time, and later repeated in maintenance periods between user runs, or even as a dedicated experiments for development of techniques. Measurement of the wavefront variation during experiments may also be possible with this device.

Single-shot λ spectrometer

Knowing the precise wavelength of each FEL pulse is particularly valuable in imaging and in nanocrystallography. The recorded diffraction patterns scale with the wavelength, and a diagnostic to determine the wavelength will aid the analysis of these patterns greatly. Furthermore, recent work suggests that the knowledge of the beam's spectrum allows for a more relaxed requirement on the temporal coherence of the FEL radiation [22], which potentially means non-monochromatised radiation could be used to image to high resolution, bringing benefits both from the increased flux and ease of operation that this entails. There are two different technologies proposed to deliver a single-shot spectrometer for X-ray FELs [55] [56], each of which differ somewhat in design. One concept proposes the use of a high-quality mirror and a perfect crystal to disperse the beam as a function of photon energy, while the other proposes to use elliptical, reflective zone plates for the same purpose. The merits of each of these methods will be evaluated during the technical design phase. It is clear that both methods, to operate at the full pulse rate of the European XFEL, require the use of at least a 1D detector that performs at the full pulse rate. A two-dimensional detector may also be used, and one "tile" (that is, a subset) of an AGIPD detector may be a possible candidate for such a device. Naturally, this is a measurement that will be made downstream of the diffraction measurements; it is ideally shot-to-shot and may even form part of the so-called "intelligent" beamstop.

"Intelligent" beamstop

The final component of the SPB instrument will be the so-called "intelligent" beamstop, potentially incorporating a solid-state flux monitor, the wavelength spectrometer, and the WMD together at the most downstream position of the hutch. A simple YAG screen will also be able to intercept the beam at the beamstop position, again predominantly for alignment purposes. Another interesting option that can be explored is the detection of emitted photoelectrons from the beam impact in a Radio Frequency (RF) cavity for timing monitoring, as it will be required for relative arrival time determination in pump-probe experiments.

Coherence monitor

A measure of the transverse coherence of the pulses is useful, for different operation modes of the machine. Such a monitor could be inserted and retracted, or installed during maintenance, and could operate by measuring the visibility of diffraction from a known structure. This monitor may only be needed intermittently, as FEL beams are expected to be [29] and have been measured to be [30] highly coherent.

Alignment laser

A simple, visible light alignment laser that can be coupled into the instrument upstream and follow the optical path of the FEL beam will be essential for pre-aligning the instrument when the FEL beam is not available. This will maximize the use of the FEL beam time, and greatly facilitate the coarse alignment of new or modified elements in the instrument. The key requirement is the easy insertion and removal of this laser or a coupling-in mirror. Two insertion locations may be relevant, one that is exclusively in the beam path of SPB, which can be used whenever beam is not in the SPB hutch, and another from much further upstream, which will always follow the beam path, but can only be used when the FEL is not in operation.

Timing monitor

A timing monitor, to find the time overlap of a pump laser and the X-ray pulse, is another useful diagnostic. It could consist of a Silicon Nitride surface that measures a change in reflectivity on a fast photodiode, as a function of time (similar to e.g. [57]).

8   Pump laser delivery

The availability of ultrabright, ultrashort pulses of X-rays gives rise to the possibility of investigating the behaviour of samples on the femtosecond timescale. In particular, so-called "pump-probe" experiments are possible, where the sample is perturbed or "pumped" with a source of radiation and the resulting state, some time delay later, is measured or "probed" with an often different source of radiation. In particular, an optical laser pump and an FEL probe are a powerful way to observe time changes in the structure of a sample triggered by the optical laser and observed with the tools of single particle imaging.

In order to enable these experiments, an optical laser—with pulse durations comparable to that of the FEL and sufficient pulse energy to excite the expected suite of samples—is required. Ideally, this laser will also operate at the 4.5 MHz intra-train repetition rate of the European XFEL.

Laser

The European XFEL will emit high rep-rate pulse bursts at 10 Hz burst rate and X-ray pulse widths down to 15 fs or even below. Off-the-shelf laser technology to match both the required pulse parameters and timing structure (pulse width and repetition rate), as well as deliver substantial pulse energy, is not available. Hence, at the beginning of 2011, the Optical Lasers group of the European XFEL (WP78) embarked on a laser development program, aiming to fill that gap. Based on non-collinear optical parametric amplification (NOPA), a first demonstration, operating continuously at up to 100 kHz, was shown at DESY in collaboration with the University of Jena and Helmholtz Institute Jena. In 2009, this system delivered in excess of 60 µJ, sub-10 fs pulses at 800 nm [58]. The development aims to scale the pulse energy and repetition rate to the mJ and MHz levels, respectively, with a timing structure matching that of the European XFEL (10 Hz train operation, up to 4.5 MHz intra-train). Due to similar laser requirements for other FELs at DESY

(FLASH II), the European XFEL and DESY laser groups have formed a collaboration to address these requirements. For the start of operation of the European XFEL in 2015, it is envisaged that the Optical Lasers group will provide 800 nm burst-mode lasers with pulse durations of around 15 fs and pulse energies of 0.1–0.2 mJ at 4.5 MHz intra-train repetition rate. Furthermore, the system should also be capable of several mJ pulse energy at a 100 kHz with a minimal degree of configuration change.

Synchronization between XFEL and laser pulses, as well as the lowest possible timing jitter and drift of the laser, are basic requirements for time-resolved, pump-probe experiments, including the time-resolved imaging of single particles and biomolecules and studies of laser-oriented molecules. The laser is to be synchronized to the XFEL timing distribution system (WP18), which has a prospective timing jitter of around 10 fs (rms) with respect to the XFEL machine clock. The laser is expected to add little to the pulse-to-pulse jitter and should therefore have the best possible synchronization with the FEL pulses. There will, however, be slow drift requiring compensation within the laser and possibly also reaching as far as the experiment chamber if drifts due to the beam delivery system are too severe. Ultimately, however, the synchronicity will of course also depend on and be determined by the timing jitter and drift of the XFEL with respect to the machine clock.

Delivery of laser radiation to the interaction region

The pump-probe laser system and its synchronization and delay control unit will be located in a laser room close to the experiment area dedicated to the SASE1 beamline. The beam will be delivered via vacuum tubes to a laser table within the SPB hutch, where specific adaptation of the laser parameters to the different experimental needs will be undertaken. This table will house the opto-mechanics and optics required to couple the laser into the SPB chamber, as well as the necessary laser diagnostics including power meters, cameras, timing drift compensation, spectrometers, and an autocorrelator. In general, this laser delivery apparatus will deliver as small a spot size as possible to the interaction region for maximum interaction with the sample. A

key design consideration of minimizing this spot size will require minimizing the f-number of the optical system delivering the beam into the interaction chamber. The spatial overlap between injected sample and optical laser will be achieved simply by observing the laser's reflection from the sample in the interaction region with a camera located in the sample chamber.

Wavelength tunability of the pump laser

The laser can be modified to provide access to wavelengths other than the 800 nm discussed above. Specifically, ultraviolet (UV) laser radiation is considered, as well as the case of tunability.

Ultraviolet (UV) radiation

The pump laser described above can be frequency tripled or even quadrupled to deliver UV radiation as a pump, albeit at reduced energies. This has to take place as close as possible to the interaction chamber, since beam delivery optics will have to be adapted accordingly.

Tunability

The ability to tune the pump laser to arbitrary wavelengths clearly opens up opportunities for a wider variety of science than fixed wavelength operation, including tuning to achieve optimal absorption in samples that may be transparent at an 800 nm wavelength. In particular, the range from ultraviolet through the infrared has been requested to be available for pumping biological samples.

Again, tuning of pulse wavelengths has to be achieved as close as possible to the experiment, as beam delivery optics will have to be adapted to the specific requirements of the experiment. One option to achieve tunability with reasonably short pulses would be to operate a Noncolinear Optical Parametric Amplifier (NOPA), pumped by the frequency-doubled (515 nm) or tripled (343 nm) ps-pump pulses of the pump-probe laser NOPA located in the laser-hutch, which are planned to be made partially accessible at the experiment. A seed for the experiment NOPA could, for instance, be derived

from the super continuum, generated by the pump pulses or by the ultrashort 800 nm pulses from the pump-probe laser.

9   Detector system

The European XFEL produces an unprecedented rate of X-ray pulses within its train structure, with individual pulses spaced 220 ns apart (that is, an intra-train repetition rate of 4.5 MHz). For experiments that collect data in two spatial dimensions on a 2D area detector, such as for single particle imaging or nano-crystallography, the data rate to be measured and recorded provides a significant technical challenge. Three detector programs designed to meet this data rate challenge are presently working towards producing 2D area detectors for the European XFEL.

Example:

www.xfel.eu/project/organization/work_packages/wp_75/2d_x_ray_detectors/

Of the three programs, two will produce detectors sensitive in the hard X-ray regime, with an optimized performance at a photon energy of 12 keV: the Large Pixel Detector (LPD) and the Adaptive Gain Integrating Pixel Detector (AGIPD). The most obvious difference to the casual observer is the pixel size: 500 μm for the LPD and 200 μm for the AGIPD. The DEPFET Sensor with Signal Compression (DSSC) detector is designed for lower photon energies and is the most relevant detector of these for the lower energy range down to 3 keV.

As discussed earlier, the (solid) angle subtended by an individual pixel must decrease to accommodate samples of increasing size. For a finite length hutch, and a detector of fixed pixel size, this bounds the maximum size of sample that can be investigated with coherent imaging. The pixel size becomes the defining criteria in choosing the AGIPD to map to the SPB instrument as its detector of choice for the harder energy range of operation.

The initial AGIPD to be delivered is to be a 1 megapixel (Mpx) device. Following some geometrical and diffraction considerations (for details, see Appendix A, "Limitations on maximum sample size", on page 81), we find that

the number of pixels in the detector limits the number of (full-period) resolution elements in a coherent imaging experiment by:

$$N_{res} = \frac{N_{detector}}{2\sigma}$$

where σ is the linear sampling ratio and the expression assumes no constraints on propagation length. This means that a 1 Mpx detector is limited to deliver about 125 resolution elements across a given sample for an experimentally reasonable sampling rate of four (4). For a small protein that is 30 nm in diameter, this corresponds to a detector limited resolution of 2.4 Å. For a large virus of 500 nm diameter, this corresponds to 4 nm. These calculations assume that the detector can be placed at the necessary propagation distance to realise the optimal sampling (and hence resolution), which may not always be convenient. For example, to reach 1 Å resolution with the 1 k x 1 k AGIPD detector, the sample-to-detector distance needs to be as short as 10 cm. To appropriately sample a 1.5 µm sample with 12 keV radiation, the sample-to-detector distance needs to be as large as 12 m. Furthermore, for a detector very close to the sample, it is not clear that the central speckles can be readily recorded there, as they may pass through the central aperture of the detector, which will be designed with a minimum size limited by the mechanics of the adjustable aperture. At present there is a fixed hole size foreseen for AGIPD, though the science will benefit from a variable sized aperture.
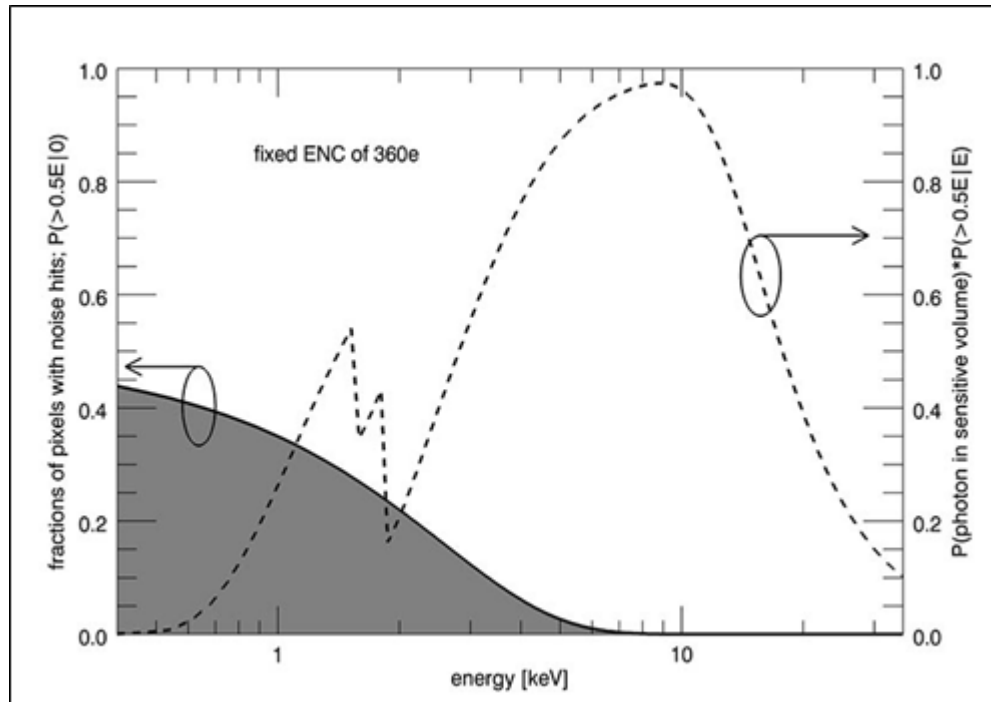
2D detectors

This section describes the expected properties of the diffraction data to be measured and from this deduces the required mechanical control, interlock system, background reduction, and wavefront monitoring associated with 2D detectors.

Diffraction data

The key properties that a 2D area detector for coherent imaging applications at the European XFEL should ideally satisfy:

- Compatibility with the 4.5 MHz repetition rate within individual pulse trains of FEL radiation.

- Ability to read out, or store for readout between trains, an entire train length (2 700 pulses) of images, a third of this number when the accelerator is multiplexing to three beamlines or as many as is technically feasible.

- High quantum efficiency across the operating range (for SPB, 3–16 keV).

- Single photon sensitivity (> 5 σ) across the operating range of the detector (that is, less than one false positive per Mpx).

- Free of external background to a level of less than one background hit per Mpx.

- High dynamic range (preferably as much as six (6) orders of magnitude [1], but as high as is practicable). This can be mitigated by the use of a second detector in a single experiment [1].

- Pixel size that allows appropriate sampling of the diffraction data for the proposed sample sizes and propagation distances (see [1], Appendix A).

- Number of pixels that is commensurate with the number of resolution elements required (i.e. at least 1k x 1k, preferably more).

- Well-calibrated (but not necessarily linear) response, which is accurate to better than Poissonian noise.

- Individually replaceable detector modules, to minimise downtime in the unfortunate event of detector damage.

- Stable pixel positions, both with time and for replaced modules.

- Acceptance of a VETO signal to reject bad frames in real time or to overwrite frames when better data arrives (that is, save the best shots).

- Radiation hard, both to single, intense shots and radiation hard after prolonged exposure to the beam in regular operation

- Adjustable sized hole that can be matched to the size of the direct beam for different beam sizes.

- In-vacuum operation that allows the direct beam to pass through the detector's central hole and propagate further downstream continuously in-vacuum.

Figure 22. *Efficiency of the AGIPD detector and fractions of pixels with false hits as a function of photon energy. This plot is an approximation based on preliminary data. (Figure courtesy of Julian Becker and Heinz Graafsma, DESY.)*

The AGIPD detector satisfactorily meets many of these requirements, especially concerning the compatibility with the repetition rate, useful pixel size, and, in part, the high dynamic range and appropriateness for the operating photon energy range of the SPB instrument.

Specifically, the AGIPD detector is being developed to deliver:

- Acquisition at 4.5 MHz rates.

- 200 μm × 200 μm pixel size.

- 1024 × 1024 pixels.

- Minimal probabilities of a false hit across part of the operating range. (Figure 22 show the probability of a false hit (as fraction of pixels with noise hits) as a function of photon energy.)

- Single photon sensitivity across part of the operating range. (Figure 22 shows single photon sensitivity as a function of energy (simplified version, does not include detector effects such as charge splitting, etc.)

- Sensor full well capacity of 1×10^4 photons per pixel/pulse at 12 keV. (Figure 23 shows the AGIPD full well capacity as a function of incident photon energy.)

- Three linear gain stages with a linearity better than 1%.

- In vacuum operation, including the possibility of passing the undiffracted beam, in-vacuum, through the detector central aperture (ideally, a resizable hole).
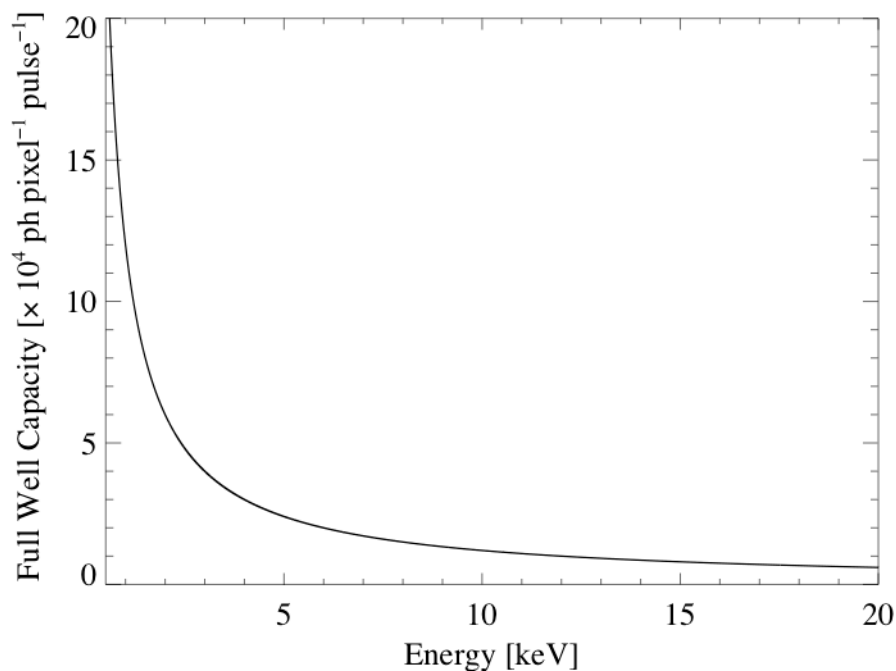
Figure 23. *Anticipated full well capacity of the AGIPD sensor as a function of incident photon energy as estimated from the 1×10^4 photons/per pixel/pulse at 12 keV specification. (Figure courtesy of Markus Kuster, European XFEL.)*

The AGIPD detector does represent some compromises from what would be an ideal detector for single particle imaging. In particular, the limited number of images stored and then read out between frames limits the maximum rate at which data can be acquired. The nominal maximum number of 300 frames

per train is almost an order of magnitude less than the maximum number of pulses the European XFEL can deliver. A second limitation is the total number of pixels in the detector, limiting the achievable resolution for samples of a given size. Additionally, the 200 μm pixel size limits the maximum size of objects that can be investigated, in a hutch of feasible length. Despite these limitations, the AGIPD detector's ability to operate at the intra-train frame rate, the possibility of vetoing frames, and the not too large pixel size, makes it the most satisfactory detector for the SPB instrument that is expected to be available for first light.

The noise floor of the AGIPD detector is potentially an issue given the 5σ requirement stated above, as it clearly falls below this for lower photon energies. This requirement will be re-examined quantitatively in light of the SPB modelling program by examining the noise tolerance of algorithms that are used to reconstruct 3D structures from very weak, single photon containing diffraction patterns, though qualitative evidence already suggests that minimizing false positives in a given frame is an important requirement of such algorithms. A further alternative may be to explore a dedicated lower energy detector for the low energy range of the instrument, though this removes some of the benefits of this range, namely to adjust the incident energy to the sample's scattering strength in-situ in real time. In that case, the additional constraint of easily switching between detectors is imposed to the mechanics of the detector mounts.

Required mechanical control

The detector will need to be compatible with traversing distances of at least tens of centimetres in-vacuum on a rail that propagates in the direction of the FEL beam, preferably a metre or three. It should be able to be relocated at positions closer and further from the interaction region on the scale of metres, with minimal intervention, to allow operation for all samples considered with only a single detector present. The detector should also be controllable to be positioned in the directions transverse to beam propagation with travel ranges of centimetres and precisions of better than a pixel. The location of each pixel in the detector will need to be calibrated with a calibration sample of known composition, such as a single crystal or powder sample.

Interlock system for detector protection

An interlock system that is integrated with the detector and beamline controls is required to protect the detector in case of unintended exposure to FEL radiation, for example the unintended illumination of strongly diffracting ice crystals.

Background reduction

For the requirements placed on the detector above to be fully exploited, the background of both X-ray and visible light reaching the detector needs to be minimized. Visible radiation can be reduced by coating the detector with a layer of Aluminium that is thick enough to absorb the visible light, but thin enough to still transport the lowest energy X-ray photons produced by the SASE1 undulator. In practice, this is readily achieved with a sub-micron layer of Aluminium. The X-ray background will be minimized by the careful use of apertures and will be explored in part through the SPB modelling program.

Wavefront monitoring

Ideally, the wavefront monitor described in the Chapter 7, "Instrument diagnostics systems", on page 55 will be able to measure at the 4.5 MHz rate of the pulse trains. This would then require a detector capable of this rate, albeit with fewer pixels than the primary detector(s) used for measuring diffraction data. A candidate for this purpose may be a detector composed of a subset of an AGIPD detector. The wavefront monitor may be composed of a traditional Hartmann-Shack sensor or, if necessary, a novel design incorporating elements of iterative phase retrieval.

1D detectors

While the primary data from the SPB instrument will be collected in 2D area detectors, as described above, secondary information may be collected in a variety of other detectors including, for example, an electron Time of Flight (eTOF) spectrometer that can be used to determine if zero, one, or multiple samples have been hit by the FEL beam, and perhaps also the composition of that sample by investigating the electron yield and spectra produced by the destroyed sample.

Optional additional detector(s)

Appendix A, "Limitations on maximum sample size", on page 81 describes the geometrical limitations on the achievable resolution that the available propagation length, the detector pixel size, and the number of pixels places on a sample of a given size. Of these three quantities, the available propagation length is limited by the length of the experiment hall, and the pixel size of the European XFEL detectors is severely limited by the required technology for storing as many images as possible from a single train of FEL pulses. The number of pixels in the AGIPD detector, however, is extensible in each direction, resulting in the possibility of a four (4) Mpx (or larger) detector. Doubling the number of pixels can improve the geometrical limit on the resolution by a factor of two, making the very-important-for-structural-biology [8] [9] sub 2 Å regime accessible for typical-sized proteins of tens of nanometres in diameter, which is of benefit both for single particle imaging and nanocrystallography.

An additional detector presents capability beyond just increasing the resolution of measured patterns in proportion to its size. A second detector downstream of the first relieves the upstream detector of needing to measure the low spatial frequency components of the diffraction data, which we know are essential to a faithful inversion to sample structure [59]. The upstream detector is then not required to measure this data close to the direct beam making the experimental realization possible in a larger space, leaving more

opportunity for novel ideas and experimental strategies in the interaction region.

AGIPD 4 Mpx

The opportunities outlined in the preceding subsection could be satisfied by a 4 Mpx version of the AGIPD detector. An additional detector not only provides the benefits of improved resolution and the opportunity to exploit a dedicated downstream diffraction measurement, it also makes the optional refocusing scheme outlined earlier possible, as a second detector would be required to run the SPB instrument with a second, parasitic interaction downstream of the primary interaction. A second detector also relieves somewhat the demand on a very high dynamic range for the case of highly scattering single particles. As the signal is to some approximation monotonically decreasing, the large dynamic range of data produced can be readily divided between an upstream and downstream detector.

An additional 2D detector at the SPB instrument represents an excellent additional capability, as it:

■ Improves the geometrically limited resolution.

■ Allows for a low resolution "back detector" that can more carefully sample the low spatial frequencies of the diffraction data.

■ Improves the dynamic range of the detector system for a given dynamic range in a single detector.

■ Improves the viability of crystallography and nano-crystallography, where accurately finding the centroid of Bragg peaks is essential to the efficacy of the method.

It would therefore be advantageous for the SPB instrument to have either a 4 Mpx detector in addition to the initial 1 Mpx device presently accounted for. An additional detector also provides a backup in case of detector maintenance. The option for this additional detector will be pursued should the required resources become available to deliver this.

10   Data acquisition, management, and analysis

This chapter provides an overview, some details, and conclusions about data acquisition (DAQ), data management (DM), and scientific computing (SC) for the SPB instrument.

Outline

The SPB instrument's data handling from acquisition and control through data management to scientific computing will be fully integrated with the hardware and software architecture framework being developed by the European XFEL DAQ/DM/SC group for use with all instruments at XFEL.

The DAQ/DM/SC system architecture foresees multiple layers. A layered architecture with well-defined interfaces increases implementation flexibility as layers can be introduced, upgraded, or removed as required. The architecture design anticipates partitioning all layers associated with single or groups of detectors into separate slices for control, readout, and processing purposes.

As shown in Figure 24, six layers are currently foreseen:

1   Front-End Electronics (FEE) that controls and captures data acquired from the detector head.

2   Front-End Interface (FEI) that interfaces detector FEEs to the timing, control, and readout systems, as well as interfaces to beamline control systems, such as motors, screen cameras, etc.

3   PC Layer receives data from detectors head FEIs, and performs data quality monitoring, formatting, and additional processing.

4 Online Storage layer provides onsite storage for data acquired, and serves data for fast processing before committing good quality data to the permanent archive.

5 Offline Storage layer provides both fast and secure storage for data and is planned to be located on the DESY site.

6 Offline Analysis Clusters (OAC) to be used for bulk data analysis of user data, i.e. the Scientific Computing (SC) facility.
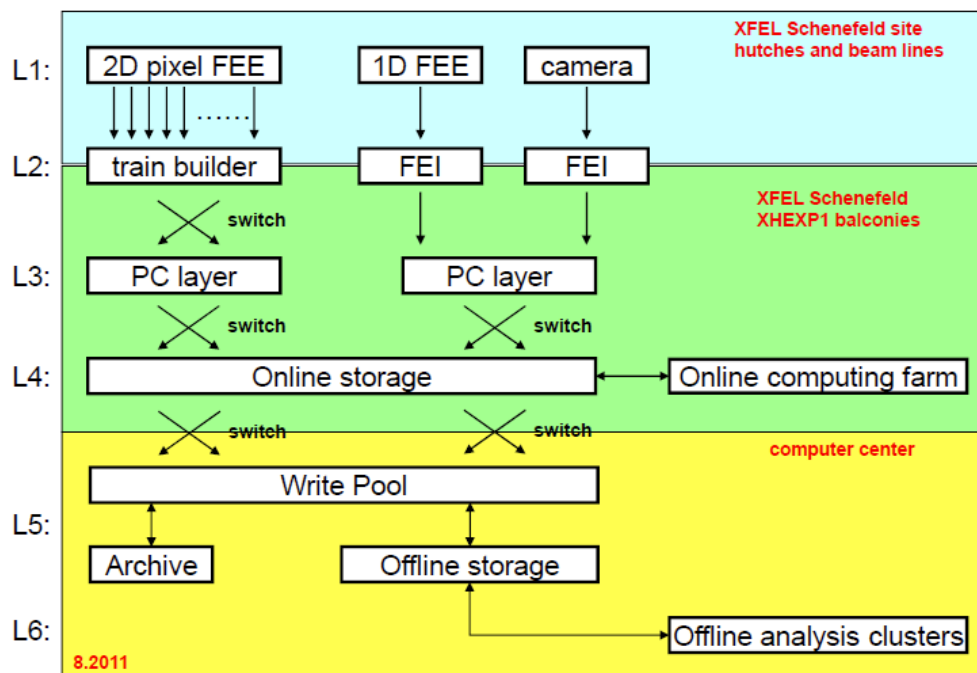
Figure 24. *Common XFEL data handling architecture*

Data acquisition

The SPB instrument, in its initial configuration, consists of a number of 4.51 MHz rep rate detectors: 1) an AGIPD 1024 x 1024 pixel 2D camera for imaging, 2) potentially, a smaller, possibly 256 x 256 pixel AGIPD type or similar European XFEL-conform, wavefront monitor, 3) a single eTOF digitizer (10 GS/s with 10-bit resolution), and 4) a single-channel APD (or perhaps multi-channel or even 2D) type fluorescent detector. The readout architecture at the European XFEL foresees that the FEE modules of these detectors are connected to a front-end readout interface that is required to

build the detector data of each pulse acquired into a complete frame and insert all frames recorded in a train (macro pulse) into a contiguous block for transfer to the PC layer. The detector-specific FEIs required by SPB will be European XFEL standards, a custom FEI (train builder) that is being developed for readout of AGIPD-type 2D pixel detectors for use at the European XFEL, and crate-based FEIs used with low multiplicity digitizer and APD readout. An MTCA4 crate APD readout system is currently being tested.

The size of detectors used can be increased by scaling the FEI implementation or adding additional readout slices as required, although a limit will eventually be reached.

The data volumes per train for the day one principle detectors are:

- AGIPD detector ASIC and FEE systems are capable of acquiring ~ 300 frames per pulse train. The 1k x 1k detectors' 2 MB frame size results in 600 MB/train, which is transferred by the train builder to PC layer blades using 10 Gbps links. The wavefront monitor's data size is 40 MB/train.

- Single digitizer digitizing the entire 600 micro-seconds of pulse train at 10 Giga Samples per second produces a data size of 9.6 MB/train. The 10 Gbps network links used can transfer 100 MB during one inter-train period, and transfer to the PC layer can be performed during the next inter-train gap without using the Round Robin approach.

- APD readout system, if only pulse height and width are required, produces relatively small amounts of data. With 2 B per value and 1 k pulses, the payload data size would be 4 kB, which is negligible compared to the above.

Data management

The extremely large data volumes generated by the detectors described above (likely at least 6 TB/day and up to 400 TB/day; see Appendix C, "Estimate of data rate", on page 90 for details), and at XFELs in general, require a paradigm change in how data and analysis are managed; storage and bulk analysis of experiment data will primarily be performed onsite with

local analysis clusters and not at the user's home institute. Consequently, centralized management services must be provided that allow this. These services include data catalogues, databases, file format implementations, user access authentication and authorization services, remote computing, etc. It should also be apparent that any storage or processing resources should be shared amongst all users. A software and hardware framework that technically implements the above features will be provided by the European XFEL.

A key feature of the data processing is that poor quality data be rejected as early as possible. In layers where conventional computing power (CPU or GPU) is present, this is performed using the framework provided by the European XFEL that allows experiment-specific software modules to be integrated and used to reject data. Additionally, a VETO system being developed for use with FEEs provides an additional rejection mechanism that alleviates the limited storage pipeline lengths associated with the sensor ASICs of the 2D detectors. The pipeline slots for bad-quality frames can be cleared for reuse by the arrival in time of a VETO signal at the FEE. The SPB instrument fluorescence APD detector will be able to provide such a signal and if no light is seen, VETO the frame. A similar VETO can be envisaged using the eTOF generated coincidence signals.

Data rejection will therefore be possible at the FEE, in the online mode on the PC layer, or just after the data is temporarily stored on the DAQ data cache. The raw data from unsuccessful experiments or from the tuning phase should not be stored in the archive. The summary information can be put to the catalogue for further reference. The reduced, good quality data will be transferred to the archive and to the highly accessible disk servers for further analysis on site in the offline mode.

It is anticipated that the SPB experiment, with potentially low target hit efficiencies, will profit significantly from the architecture design requirement that the rejection of poor quality data at all layers as early as possible should be targeted. This is especially valid as the detector only has the capability to store approximately 300 frames per train, compared with the 2 700 pulses delivered per train.

Scientific computing

The European XFEL will provide a user-friendly and fully integrated scientific computing facility that will run on onsite hardware. A major element of the scientific computing solution is the development of a software framework and toolkit that will be used in all layers from scientific computing and data storage to detector and beamline control. The framework is designed to be extremely flexible and allows, with negligible restrictions on the software technology or platform preferences, the integration of complete external applications, allowing users to incorporate their own analysis software into the European XFEL framework should they so wish. The framework provides a complete suite of tools including configuration, Message Oriented Middleware, database access, process pipelining, bindings to other languages, a scriptable application interface as well as a GUI system. The scientific computing system being developed by the European XFEL will exploit this framework to expedite user analysis of data. The SPB instrument group and interested experimenters will participate strongly in its development, including in the development and implementation of the relevant analysis software.

Conclusions

The data handling and analysis requirements of the SPB instrument described can be satisfied by the hardware and software architecture framework being developed.

11   Conclusions and outlook

In summary, the requirements of the SPB instrument, as defined by community consultation at the SPB workshop of 2008 and outlined in the subsequent report [1], are satisfied by the optical design presented in this conceptual design report. In particular, the use of metal-coated KB mirrors as focusing optics, or derivatives thereof, allow for high transmission, minimal wavefront error, appropriate focal spot sizes, long depths of focus, and a broad range of operating photon energies. One question that remains to be confirmed is the damage behaviour of these mirrors at the expected fluences, though today's best estimates suggest that any adverse effects are unlikely.

The optimal detection system has an upstream and downstream pixel detector to allow the measurement of high scattering angles, and hence high resolution information as well as prudently sampling the low frequency information near to the beam at a higher rate, which provides a powerful drive for the convergence of iterative reconstruction methods.

The question of precisely at what rate false hits in a detector cause algorithms that reconstruct weak, single-photon-in-a-pixel-containing diffraction patterns will be explored within the SPB modeling program, to inform the tightening or relaxing of constraints on the detector development program. A value of 5σ is the best estimate to date.

The technical design phase will see question of the optimal and precise geometrical design explored, such as whether an XGMD can be placed between the focusing mirrors and the interaction region, though the broad outline given here already demonstrates the proposed outline of the instrument.

The next phase of development will also explore the optimal operating parameters of the SPB instrument, taking into account source parameters, beamline transmission, estimated sample scattering and detector response. This will allow the identification of a so-called "window of opportunity" in which the SPB instrument can optimally operate. In particular, the technical design

report will explore detection at the lower photon energy range of the instrument, the scientific value of a monochromator, and the relationship between sample size and optimal beam size. These points, identified by the ART and the Scientific Advisory Committee (SAC) of the European XFEL and appreciated by the SPB team, are among a number of scientific design questions that form the next steps for the SPB instrument design process, and are planned to be investigated in the near future.

In conclusion, the design described herein and the route through the technical design phase proposed will allow the SPB instrument of the European XFEL to perform coherent diffraction experiments on the three canonical classes of sample: weak scattering single molecules, nanocrystals and other ordered material, and more strongly scattering samples, such as cells, viruses, and materials science samples. The design also does not preclude further varieties of coherent imaging experiments to be performed. With continued progress the SPB instrument can conceivably aim to be the premier destination in the world for the imaging of single particles, clusters, and biomolecules with X-ray free-electron laser radiation.

A Limitations on maximum sample size

This appendix describes the limitations on the maximum size of samples that can be investigated using the SPB instrument.

Sampling considerations

The available propagation length in the hutch, combined with the pixel size of the detector and the wavelength of the incident radiation, puts a constraint on the maximum size of samples that can be investigated. Here, we assume that the available space from the sample to the detector in the SPB hutch, in the direction of beam propagation, is approximately 8 m with a detector pixel size of 200 µm square for operating photon energies of the SPB instrument from 3 keV to 16 keV. The linear sampling ratio σ, i.e. the number of pixels per fringe (or speckle) in one dimension is taken to be four (4), in good agreement with experimentally realized values.

We further define z as the sample-to-detector-distance, λ as the photon wavelength, and Δx as the detector pixel width. Assuming elastic scattering, the photon scattering vector **q** has a modulus

$$q(\theta) = \frac{4\pi}{\lambda} \sin\theta$$

where θ denotes the half-diffraction angle. The distance q corresponds in real space to a full period length d via q = 2π/d. Accordingly, the above equation can be written as

$$\lambda = 2d(\theta) \sin\theta.$$

The detector sampling becomes most critical for large objects, which cause small speckles, and thus require the detector to be as far away from the sample as the geometry allows. In this limit of small diffraction angles the

latter equation implies (for the largest diffraction angle to be covered by the detector at distance z):

$$\lambda \cong d_{res} \sin 2\theta = d_{res} \frac{N\Delta x}{2z}$$

with d_{res} denoting the smallest resolvable spatial period in real space and N denoting the number of pixels on the detector in one Cartesian coordinate direction. In addition, a single speckle, sampled with σ detector pixels corresponds to the linear extension D of the sample in real space, i.e.

$$\lambda = D \frac{\sigma \Delta x}{z}.$$

Combining the last two equations and letting $N_{res} = D/d_{res}$ denote the number of (full-period) resolution elements within the linear extension of the sample, one arrives at

$$N_{res} = \frac{N}{2\sigma}.$$

As a consequence, for a given sampling ratio of e.g. $\sigma = 4$, the sample contains—independent of wavelength and geometry— 125 (full-period) resolution elements along one dimension.

As an example let $\lambda = 1$ Å, z = 8 m, $\Delta x = 200$ μm and $\sigma = 4$. The maximum extent of the sample is then required to be smaller than 1 μm, which is adequate for viruses and smaller particles but usually not for biological cells and even many organelles. Thus, for an object of 1 μm in size the limit to the resolution given by the number of detector pixels and the geometry is 8 nm.

If we now consider the scenario at the lowest energy end of the instrument's operation, 4 Å (~3 keV), we can improve the size of samples we can investigate, at the expense of resolution. This scales linearly, so we find that, at 3 keV, we can investigate samples up to 4 μm to a resolution of about 32 nm for the propagation distance, pixel size and sampling described above.

From this, we see that an 8 m propagation length between sample and detector is really at the shortest scale of acceptability for larger samples, and the SPB instrument (and its users) would benefit from an even longer propagation distance. A small (4 m) increase would provide a greatly

improved situation for larger samples, increasing the attainable sizes by 50%. Present planning for the SPB instrument considers the most likely available propagation distance to be 10 m.

For smaller samples, such as single molecules of tens of nanometres in size, this limitation is not critical. If we consider a "larger" molecule of 50 nm in diameter, we find that, for λ = 1 Å, z = 40 cm is adequate for such a sample and the resolution extends to 4 Å. The geometrically limited resolution improves commensurately with increasingly smaller samples, and for more typical single molecules of 25–30 nm size approaches a value of about 2 Å. The number of pixels in the detector limits this resolution as we approach larger samples sizes. This point is discussed in Chapter 9, "Detector system", on page 65.

Table A-1. Geometrically limited (full period) resolution and required sample-to-detector propagation lengths for a variety of sample sizes and incident photon energies and a linear sampling rate of 4.

Sample max. dimension [nm]	λ [Å]	Photon energy [keV]	Geometrically limited resolution [Å]	Required propagation distance [m]	Minimum hutch length (baseline) [m]	Minimum hutch length (refocusing) [m]
20	0.8	15.4875	1.6	0.20	10.20	14.20
30	0.8	15.4875	2.4	0.30	10.30	14.30
30	1	12.39	2.4	0.24	10.24	14.24
100	1	12.39	8	0.8	10.80	14.80
500	1	12.39	40	4.00	14.00	18.00
500	2	6.195	40	2.00	12.00	16.00
1 000	1	12.39	80	8.00	18.00	22.00
1500	2	6.195	120	6.00	16.00	20.00
2 000	4	3.0975	160	4.00	14.00	18.00
3 000	4	3.0975	240	4.00	14.00	18.00
1 500	1	12.39	120	12.00	22.00	26.00

The numbers in Table A-1 can be improved in a number of ways. A detector with a greater number of pixels will increase the attainable resolution. One can also relax the requirement on the linear sampling ratio to the theoretical minimum [60] for an improvement of a little more than a factor of 2. A further way to increase the geometrically limited resolution by about a factor of 2 is to align the detector such that the direct beam does not pass through its centre, but rather at one side or at one corner, increasing the resolution respectively in one or both dimensions by a factor of 2; however, the impact of this on composing and reconstructing data in this way has not yet been studied.

B   Sundry optical layouts

This appendix outlines alternative ways to deliver the optical needs of the SPB instrument, though these are not as attractive as the mirror solution outlined in the main text mainly due to throughput or background considerations. These alternatives do, however, offer plausible optical layouts for the SPB instrument in the unlikely event that the simulations and/or measurements of damage to the metal-coated (or SiC-on-metal-coated) mirror solution are higher than we expect due to our best knowledge today.

Alternative optics for the 1 μm focal spot

This section describes three optical layout alternatives for the 1 μm focal spot.

Alternative 1: Mirrors without metal coating

Minimizing distortions to the wavefront of the FEL pulses is essential to the optimal exploitation of the coherent properties of that radiation for FEL-based coherent imaging [10]. Alternative 1 is an entirely mirror-based solution that combines the fewest number of high-efficiency focusing elements with minimal aberrations. The key drawback of this approach is the limited aperture of the non-metal coated Kirkpatrick-Baez (KB) mirrors in the hutch. This, combined with the large size (up to 5.5 mm) of the beam at the low energy range, means that a significant amount of intensity will be lost at the entrance plane of the optics. Diffraction effects from the finite aperture of the mirrors will also produce intensity variations across the focused beam. One dimension (horizontal) can be mitigated here by focusing the beam with the second offset mirror [23]; however, the beam transport optics do not present an option to focus in the vertical direction. One mitigation of this could be to use mirrors with more than one stripe of coating, for example one metal and one non-metal coating.

Variation 1(a): Kirkpatrick-Baez mirrors

The simplest and least technically demanding variation is to use existing KB mirror technology with Carbon, Boron Carbide, or Silicon Carbide coatings, extended in length from existing implementations as much as technically possible to accept as large a fraction of the incoming beam as possible. The current goal for this length is 800 mm, as described for the offset mirrors in the X-Ray Beam Transport conceptual design report [23]. The mirrors may be bendable to allow variation of the spot size delivered to the interaction region to vary (at the expense of defocus), and would be coated with carbon to improve their reflectivity in the SPB wavelength range. The bend would also allow these mirrors to serve as pre-focusing mirrors for the sub-100 nm optics while maintaining the same focal plane.

Variation 1(b): Kirkpatrick-Baez mirrors with adaptive optics

Adaptive Optics (AO) may additionally be applied to mirrors to correct for imperfections in figure error, reducing the tolerances on mirror manufacture and perhaps opening the way to implementing mirrors even longer than 800 mm. Adaptive X-ray optics have been demonstrated for shorter mirrors at synchrotron sources [61]. Present technology does not permit the construction of adaptive mirrors that are cooled to the tolerances required here, though the development of this technology will be observed throughout the technical design phase for any significant improvements.

Variation 1(c): Kirkpatrick-Baez mirrors with multilayer coatings

The use of multilayer optics is, in principle, possible for the parameters of the SPB instrument; however, the strong dependence on the incident angle required as a function of energy makes these types of mirrors less practical than those described earlier, particularly from a day-to-day operation point of view. Similarly to variation 1(b), the progress in this technology will be closely followed during the technical design phase.

Alternative 2: Vertical collimation

Alternative 2 is similar to Alternative 1 and the primary optical design presented in the main text, except that a vertical collimating element is inserted at a distance 230 m from the source. The performance of the instrument will depend heavily on the nature of this collimation element.

Ideally, for easy switching between Alternative 1 and 2, the collimating element should not change the optical axis of the beam—especially when placed well upstream. Furthermore, as the beam will traverse many optical elements and diagnostics between the collimation and the experiment station, care will need to be taken to confirm that these elements will not be subject to radiation damage at the higher flux density that comes with a collimated beam.

Variation 2(a): Large aperture focusing mirror collimation

The best general solution that combines minimal wavefront disturbance with high throughput is to use KB focusing mirrors with a two-mirror vertical collimation optic upstream of the SPB hutch. This would maintain all the advantages of a mirror-only focusing solution, while collecting a larger fraction of the beam to focus. The second mirror would be bendable to account for the different possible source points in different modes of operation so the beam can be focused into a single plane independent of photon energy. This mirror system might benefit from Alternatives 1(a) and 1(b) if deemed feasible, though, at this point in time, the preferred option at 230 m upstream is carbon-coated mirrors that are 800 mm in length.

Variation 2(b): 1D diamond Fresnel zone plate collimator

A Fresnel zone plate (FZP) is an economical and high-quality optic that functions on axis and would produce minimal wavefront distortions to the beam. The drawback of such a focusing optic is the relatively low efficiency of a FZP when compared with other focusing elements. While an efficiency as high as 20% is possible, typically zone plates are 10% efficient, which is a significant limitation to the usefulness of FZPs. Furthermore, zone plates are chromatic, meaning a variety of different FZPs would be required to span the operating wavelength range of the SPB instrument.

Variation 2(c): 1D compound refractive lens collimator

Compound refractive lenses (CRLs) are also an economical, on-axis optic that could be inserted into the beam path or removed as necessary. Like FZPs, CRLs are chromatic elements, and a selection of elements would be required to match the required focal length across the range of X-ray energies at the instrument. They are expected to be viable (from a damage point of

view) for the unfocused FEL beam. Furthermore, to date, compound refractive lenses (CRLs) deliver ultrasmall-angle scattering signal from grains in the materials from which they are constructed to the focal area. As such, they are unsuitable for single molecule imaging, but plausible for nanocrystallography experiments [12].

Alternative 3: Compound refractive lenses

For a subset of sample types that do not suffer from an ultrasmall-angle scattering background, in particular nanocrystals, CRLs may be a practical alternative for collimating the hard X-ray beam to maximize the flux at the sample. While not necessarily ideal for single molecule experiments, CRLs are an inexpensive, easy to use, on-axis optical element that could be readily used for nano-crystallography experiments. Alternative 3 utilizes CRLs exclusively for that application, including for the vertical collimation in the tunnel (at ~ 230 m from the source) and for the focusing optics in the experiment station. It is envisaged that, in the focused FEL beam, below ~ 7 keV, Beryllium CRLs will melt for reasonable flux densities [23], and care must be taken to avoid this case. A complete CRL system is considered as a relatively low cost additional optical system that could be inserted and removed from the optical path, as necessary. This alternative is a candidate to be installed alongside the primary system due to the inexpensive and relatively compact nature of CRLs.

Alternative optics for the sub-100 nm focal spot

This section describes one optical layout alternative for the sub-100 nm focal spot

Alternative: Fresnel zone plates

Other focusing options, such as diamond Fresnel zone plates (FZPs), will be considered as alternate solutions, but due to limitations, such as their limited working distance and efficiency, they do not necessarily represent an ideal solution for the instrument. FZPs may represent the best, budget-conscious design for the sub-100 nm optics, combining quality wavefront properties with relatively low cost at the expense of efficiency.

Alternative for the refocused focal spot

This section describes one optical layout alternative for the refocused focal spot

Alternative: Kirkpatrick-Baez mirrors

Kirkpatrick-Baez (KB) mirrors have all the optical advantages listed in the earlier mirror sections, but the key disadvantage of a significant length in a region of the experiment where space is at a premium.

Conclusions

The clear preference is for the metal on mirror solution as proposed in the main text. Should it be deemed that the materials are inadequate for the expected fluences, or later damage experiments demonstrate that the damage threshold is relevant to that mirror design, the alternatives presented in this appendix provide routes to an alternate optical design.

C   Estimate of data rate

A simple and brief estimate of the data rate to be measured at the SPB instrument is given in this appendix. The upper bound is given by detector. The AGIPD detector is expected to be able to measure ~ 300 frames / 0.1 s. If we consider each frame to be a 1 Mpx image (at 2 MB per image), measured continuously for a 24-hour shift in a given day, and that 80% of the available time is spent measuring, this implies that 400 TB / day of data would be measured. In practice, today's data rates are much lower than 100%. A lower bound can be given using present experience from LCLS and FLASH. For both liquid and aerosol injectors, we expect at least 100 frames/s at European XFEL repetition rates, and more likely closer to an average 1 000 frames/s.

Assuming a 30% measurement time—which corresponds with today's ratios of measurement times at, for example, a synchrotron Small Angle X-ray Scattering (SAXS) beamline or at recent FEL experiments—we see that this amounts to a minimum of about 6 TB / day and a best estimate to date of 60 TB / day. The reality may be higher still, as injection technology has improved enormously in the past few years and can be expected to continue to improve and provide higher hit rates than today. New ideas in data analysis, including the possibility of analysing multiple nanocrystals illuminated in a single shot, may lead to higher sample densities being injected and quantum leaps in the hit rate. The values quoted will also increase commensurately with area detected and should be multiplied by two (2) for the case of two (2) AGIPD detectors and by five (5) for one 1 Mpx detector and one 4 Mpx detector.

D   Abbreviations

AGIPD	Adaptive Gain Integrating Pixel Detector
AO	Adaptive Optics
ART	advisory review team
BPM	beam position monitor
CDR	conceptual design report
CFEL	Centre for Free-Electron Laser Science
CRL	compound refractive lens
CXI	Coherent X-ray Imaging
DEPFET	depleted P-channel field effect transistor
DESY	Deutsches Elektronen-Synchrotron
EMBL	European Molecular Biology Laboratory
FCDI	Fresnel Coherent Diffractive Imaging
FEL	free-electron laser
FZP	Fresnel zone plate
HDF5	Hierarchical Data Format 5
HOM	horizontal offset mirror
HORUS	HPAD Output Response Function Simulator
IMETUM	Institute of Medical Engineering, Technische Universität München
KB mirror	Kirkpatrick-Baez mirror
S2E simulation	start-to-end simulation
SAXS	Small Angle X-ray Scattering
SFX	Serial Femtosecond Crystallography
SPB instrument	Single Particles, Clusters and Biomolecules scientific instrument
SRWLib	Cross-platform, wave-optics software used here to simulate the focal properties of the SPB instrument
TDR	technical design report
WMD	wavefront measurement device
XGMD	X-ray Gas Monitor Detector

E   References

1. Mancuso, A.P., Chapman, H.N.: "Report from 'International workshop on science with and instrumentation for ultrafast coherent diffraction imaging of Single Particles, clusters and Biomolecules (SPB) at the European XFEL'", (accessed January 2008), available at: http://www.xfel.eu/events/workshops/2008/spb_workshop_2008

2. Barty, A., Boutet, S., Bogan, M.J., Hau-Riege, S., Marchesini, S., Sokolowski-Tinten, K., Stojanovic, N., Tobey, R., Ehrke, H., Cavalleri, A., Dusterer, S., Frank, M., Bajt, S., Woods, B.W., Seibert, M.M., Hajdu, J., Treusch, R., Chapman, H.N.: "Ultrafast single-shot diffraction imaging of nanoscale dynamics", Nat. Phot. 2(7), 415-419 (2008))

3. M. Altarelli et al. (eds.): "European XFEL Technical Design Report", (accessed January 2008), available at: http://www.xfel.eu/documents/technical_documents

4. Emma, P., Akre, R., Arthur, J., Bionta, R., Bostedt, C., Bozek, J., Brachmann, A., et al.: "First lasing and operation of an angstrom-wavelength free-electron laser", Nat. Photon. 4(9), 641-647 (2010)

5. SACLA, Japan. (Accessed January 2012), available at: http://xfel.riken.jp/eng/index.html

6. Fung, R., Shneerson, V., Saldin, D.K., Ourmazd, A.: "Structure from fleeting illumination of faint spinning objects in flight", Nat. Phys. 5(1), 64-67 (2009)

7. Loh, N.-T., Elser, V.: "Reconstruction algorithm for single-particle diffraction imaging experiments", Phys. Rev. E 80(2), 026705-026705 (2009)

8. Langer, G., Cohen, S.X., Lamzin, V.S., Perrakis, A.: "Automated macromolecular model building for X-ray crystallography using ARP/wARP version 7", Nat. Protocols 3(7), 1171-1179 (2008)

9. Gilmore, C.J.: "Direct methods and protein crystallography at low resolution", Acta Cryst. D 56(10), 1205-1214 (2000)

10. Mancuso, A.P., Gorniak, T., Staier, F., Yefanov, O.M., Barth, R., Christophis, C., Reime, B., Gulden, J., Singer, A., Pettit, M.E., Nisius, T., Wilhein, T., Gutt, C., Grübel, G., Guerassimova, N., Treusch, R., Feldhaus, J., Eisebitt, S., Weckert, E., Grunze, M., Rosenhahn, A., Vartanyants, I.A.: "Coherent imaging of biological samples with femtosecond pulses at the free-electron laser FLASH", New J. Phys. 12(3), 035003-035003 (2010)

11. Schropp, A., Boye, P., Feldkamp, J.M., Hoppe, R., Patommel, J., Samberg, D., Stephan, S., Giewekemeyer, K., Wilke, R.N., Saldittt, T., Gulden, J., Mancuso, A.P., Vartanyants, I.A., Weckert, E., Schöder, S., Burghammer, M., Schroer, C.G.: "Hard x-ray nanobeam characterization by coherent diffraction microscopy", Appl. Phys. Lett. 96(9), 091102 (2010)

12. Chapman, H.N., Fromme, P., Barty, A., White, T.A., Kirian, R.A. Aquila, A., Hunter, M.S., Schulz, J., DePonte, D.P., Weierstall, U., Doak, R.B., Maia, F.R.N.C., Martin, A.V., Schlichting, I., Lomb, L., Coppola, N., Shoeman, R.L., Epp, S.W., Hartmann, R., Rolles, D., Rudenko, A., Foucar, L., Kimmel, N., Weidenspointner, G., Holl, P., Liang, M., Barthelmess, M., Caleman, C., Boutet, S., Bogan, M.J., Krzywinski, J., Bostedt, C., Bajt, S., Gumprecht, L., Rudek, B., Erk, B., Schmidt, C., Homke, A., Reich, C., Pietschner, D., Struder, L., Hauser, G., Gorke, H., Ullrich, J., Herrmann, S., Schaller, G., Schopper, F., Soltau, H., Kuhnel, K.-U., Messerschmidt, M., Bozek, J., Hau-Riege, S., Frank, M., Hampton, C., Sierra, R., Starodub, D., Williams, G., Hajdu, J., Timneanu, N., Seibert, M.M., Andreasson, J., Rocker, A., Jonsson, O., Svenda, M., Stern, S., Nass, K., Andritschke, R., Schroter, C.-D., Krasniqi, F., Bott, M., Schmidt, K.E., Wang, X., Grotjohann, I., Holton, J.M., Barends, T.R.M., Neutze, R., Marchesini, S., Fromme, R., Schorb, S., Rupp, D., Adolph, M., Gorkhover, T., Andersson, I., Hirsemann, H., Potdevin, G., Graafsma, H., Nilsson, B., Spence, J.C.H.: "Femtosecond X-ray protein nanocrystallography", Nature 470(7332), 73-77 (2011)

13. White, T.A., et al.: submitted

14. Robinson, I.K., Vartanyants, I.A., Williams, G.J., Pfeifer, M.A., Pitney, J.A.: "Reconstruction of the Shapes of Gold Nanocrystals Using Coherent X-Ray Diffraction", Phys. Rev. Lett. 87(19), 195505 (2001)

15. Rout, M.P., Aitchison, J.D., Suprapto, A., Hjertaas, K., Zhao, Y., Chait, B.T.: "The Yeast Nuclear Pore Complex", J. Cell Biol. 148(4), 635-652 (2000)

16. Rosenhahn, A., Staier, F., Nisius, T., Schäfer, D., Barth, R., Christophis, C., Stadler, L.-M., Streit-Nierobisch, S., Gutt, C., Mancuso, A., Schropp, A., Gulden, J., Reime, B., Feldhaus, J., Weckert, E., Pfau, B., Günther, C.M., Könnecke, R., Eisebitt, S., Martins, M., Faatz, B., Guerassimova, N., Honkavaara, K., Treusch, R., Saldin, E., Schreiber, S., Schneidmiller, E.A., Yurkov, M.A., Vartanyants, I.A., Grübel, G., Grunze, M., Wilhein, T.: "Digital In-line Holography with femtosecond VUV radiation provided by the free-electron laser FLASH", Opt. Express 17(10), 8220-8228 (2009)

17. Giewekemeyer, K., Krüger, S.P., Kalbfleisch, S., Bartels, M., Beta, C., Salditt, T.: "X-ray propagation microscopy of biological cells using waveguides as a quasipoint source", Phys. Rev. A 83, 023804 (2011)

18. Schlotter, W.F., Rick, R., Chen, K., Scherz, A., Stöhr, J., Lüning, J., Eisebitt, S., Günther, C., Eberhardt, W., Hellwig, O., McNulty, I.: "Multiple reference Fourier transform holography with soft x rays", Appl. Phys. Lett. 89(16), 163112 (2006)

19. Williams, G.J., Quiney, H.M., Dhal, B.B., Tran, C.Q., Nugent, K.A., Peele, A.G., Paterson, D., de Jonge, M.D.: "Fresnel Coherent Diffractive Imaging", Phys. Rev. Lett. 97(2), 025506 (2006)

20. Putkunz, C.T., Clark, J.N., Vine, D.J., Williams, G.J., Pfeifer, M.A., Balaur, E., McNulty, I., Nugent, K.A., Peele, A.G.: "Phase-Diverse Coherent Diffractive Imaging: High Sensitivity with Low Dose", Phys. Rev. Lett. 106(1), 013903 (2011)

21. Whitehead, L.W., Williams, G.J., Quiney, H.M., Vine, D.J., Dilanian, R.A., Flewett, S., Nugent, K.A., Peele, A.G., Balaur, E., McNulty, I.: "Diffractive Imaging Using Partially Coherent X Rays. Phys. Rev. Lett", 103(24), 243902 (2009)

22. Abbey, B., Whitehead, L.W., Quiney, H.M., Vine, D.J., Cadenazzi, G.A., Henderson, C.A., Nugent, K.A., Balaur, E., Putkunz, C.T., Peele, A.G., Williams, G.J., McNulty, I.: "Lensless imaging using broadband X-ray sources", Nat. Phot. 5(7), 420-424 (2011)

23. Sinn, H., Gaudin, J., Samoylova, L., Trapp, A., Galasso, G.: "Conceptual Design Report: X-Ray Optics and Beam Transport", (accessed January 2011), available at: http://www.xfel.eu/documents/technical_documents

24. Tschentscher, T.: "Layout of the X-Ray Systems at the European XFEL", (accessed January 2011), available at: http://www.xfel.eu/documents/technical_documents

25. Neutze, R., Wouts, R., van der Spoel, D., Weckert, E., Hajdu, J.: "Potential for biomolecular imaging with femtosecond X-ray pulses", Nature 406(6797), 752-757 (2000)

26. Quiney, H.M., Nugent, K.A.: "Biomolecular imaging and electronic damage using X-ray free-electron lasers", Nat. Phys. 7(2), 142-146 (2011)

27. Barty, A., Caleman, C., Aquila, A., Timneanu, N., Lomb, L., White, T.A., Andreasson, J., Arnlund, D., Bajt, S., Barends, T.R.M., Barthelmess, M., Bogan, M.J., Bostedt, C., Bozek, J.D., Coffee, R., Coppola, N., Davidsson, J., DePonte, D.P., Doak, R.B., Ekeberg, T., Elser, V., Epp, S.W., Erk, B., Fleckenstein, H., Foucar, L., Fromme, P., Graafsma, H., Gumprecht, L., Hajdu, J., Hampton, C.Y., Hartmann, R., Hartmann, A., Hauser, G., Hirsemann, H., Holl, P., Hunter, M.S., Johansson, L., Kassemeyer, S., Kimmel, N., Kirian, R.A., Liang, M., Maia, F.R.N.C., Malmerberg, E., Marchesini, S., Martin, A.V., Nass, K., Neutze, R., Reich, C., Rolles, D., Rudek, B., Rudenko, A., Scott, H., Schlichting, I., Schulz, J., Seibert, M.M., Shoeman, R.L., Sierra, R.G., Soltau, H., Spence, J.C.H., Stellato, F., Stern, S., Struder, L., Ullrich, J., Wang, X., Weidenspointner, G., Weierstall, U., Wunderer, C.W., Chapman, H.N.: "Self-terminating diffraction gates femtosecond X-ray nanocrystallography measurements", Nat. Phot. 6(1), 35-40 (2012)

28. Samoylova, L., Buzmakov, A., Geloni, G., Chubar, O., Sinn, H.: "Cross-platform wave optics software for XFEL applications", Proc. SPIE 8141(1), 81410A (2011)

29. Schneidmiller, E., Yurkov, M.V.: "Photon beam properties at the European XFEL (December 2010 revision)", Preprint DESY 11-152 (2011)

30. Vartanyants, I.A., Singer, A., Mancuso, A.P., Yefanov, O.M., Sakdinawat, A., Liu, Y., Bang, E., Williams, G.J., Cadenazzi, G., Abbey, B., Sinn, H., Attwood, D., Nugent, K.A., Weckert, E., Wang, T., Zhu, D., Wu, B., Graves, C., Scherz, A., Turner, J.J., Schlotter, W.F., Messerschmidt, M., Lüning, J., Acremann, Y., Heimann, P., Mancini, D.C., Joshi, V., Krzywinski, J., Soufli, R., Fernandez-Perea, M., Hau-Riege, S., Peele, A.G., Feng, Y., Krupin, O., Moeller, S., Wurth, W.: "Coherence Properties of Individual Femtosecond Pulses of an X-Ray Free-Electron Laser", Phys. Rev. Lett. 107(14), 144801 (2011)

31. Son, S.-K., Young, L., Santra, R.: "Impact of hollow-atom formation on coherent x-ray scattering at high intensity", Phys. Rev. A 83(3), 033402 (2011)

32. The HDF5 Group, (accessed 2012), available at: http://www.hdfgroup.org/HDF5/

33. Potdevin, G., Trunk, U., Graafsma, H.: "HORUS, an HPAD X-ray detector simulation program", J. Instrum. 4(09), P09010 (2009)

34. Becker, J.: "HORUS - A detector simulation tool", XFEL seminar talk, 3.3.2011, (accessed January 2011), available at: http://hasylab.desy.de/instrumentation/detectors/projects/agipd/horus/index_eng.html

35. Pivovaroff, M., Hau-Riege, S.: Personal Communication

36. European XFEL GmbH: "First Call for Expressions of Interest in the Formation of User Consortia", (accessed 2011), available at: http://www.xfel.eu/organization/calls_for_expressions_of_interest/user_consortia

37. Deponte, D.P., Mckeown, J.T., Weierstall, U., Doak, R.B., Spence, J.C.H.: "Towards ETEM serial crystallography: Electron diffraction from liquid jets", Ultramicroscopy 111(7), 824-827 (2011)

38. Gañán-Calvo, A.M.: "Unconditional jetting", Phys. Rev. E 78(2), 026304 (2008)

39. DePonte, D.P., Weierstall, U., Schmidt, K., Warner, J., Starodub, D., Spence, J.C.H., Doak, R.B.: "Gas dynamic virtual nozzle for generation of microscopic droplet streams", J. Phys. D: Appl. Phys. 41(19), 195505 (2008)

40. Gañán-Calvo, A.M., DePonte, D.P., Herrada, M.A., Spence, J.C.H., Weierstall, U., Doak, R.B.: "Liquid Capillary Micro/Nanojets in Free-Jet Expansion", Small 6(7), 822-824 (2010)

41. Bogan, M.J., Boutet, S., Chapman, H.N., Marchesini, S., Barty, A., Benner, W.H., Rohner, U., Frank, M., Hau-Riege, S.P., Bajt, S., Woods, B., Seibert, M.M., Iwan, B., Timneanu, N., Hajdu, J., Schulz, J.: "Aerosol Imaging with a Soft X-Ray Free Electron Laser", Aerosol Sci. Tech. 44(3), i-vi (2010)

42. Benner, W.H., Bogan, M.J., Rohner, U., Boutet, S., Woods, B., Frank, M.: "Non-destructive characterization and alignment of aerodynamically focused particle beams using single particle charge detection", J. Aerosol Sci. 39(11), 917-928 (2008)

43. Liu, P., Ziemann, P.J., Kittelson, D.B., McMurry, P.H.: "Generating Particle Beams of Controlled Dimensions and Divergence: I. Theory of Particle Motion in Aerodynamic Lenses and Nozzle Expansions", Aerosol Sci. Tech. 22(3), 293-313 (1995)

44. Kewish, C.M., Thibault, P., Bunk, O., Pfeiffer, F.: "The potential for two-dimensional crystallography of membrane proteins at future x-ray free-electron laser sources", New J. Phys. 12(3), 035005 (2010)

45. Lima, E., Wiegart, L., Pernot, P., Howells, M., Timmins, J., Zontone, F., Madsen, A.: "Cryogenic X-Ray Diffraction Microscopy for Biological Samples", Phys. Rev. Lett. 103(19), 198102 (2009)

46. Huang, X., Miao, H., Nelson, J., Turner, J., Steinbrener, J., Shapiro, D., Kirz, J., Jacobsen, C.: "Anti-contamination device for cryogenic soft X-ray diffraction microscopy", Nucl. Instrum. Meth. A 638, 171 (2011)

47. Filsinger, F., Küpper, J., Meijer, G., Hansen, J. L., Maurer, J., Nielsen, J. H., Holmegaard, L., Stapelfeldt, H.: "Pure Samples of Individual Conformers: The Separation of Stereoisomers of Complex Molecules Using Electric Fields", Angew. Chemie Int. Ed. 48(37), 6900-6902 (2009)

48. Filsinger, F., Erlekam, U., von Helden, G., Küpper, J., Meijer, G.: "Selector for Structural Isomers of Neutral Molecules", Phys. Rev. Lett. 100(13), 133003 (2008)

49. Sachwitz, M., Hofmann, A., Pauliuk, S., Tiedtke, K., Wabnitz, H.: "Ionization Profile Monitor to Determine Spatial and Angular Stability of FEL Radiation of FLASH", in : Proceedings of EPAC08, Genoa, Italy, p.TUPC090 (2008)

50. Crytur Ltd. (CZ). (Accessed January 2012), available at: http://www.crytur.cz

51. Tiedtke, K., Feldhaus, J., Hahn, U., Jastrow, U., Nunez, T., Tschentscher, T., Bobashev, S.V., Sorokin, A.A., Hastings, J.B., Möller, S., Cibik, L., Gottwald, A., Hoehl, A., Kroth, U., Krumrey, M., Schöppe, H., Ulm, G., Richter, M.: "Gas detectors for x-ray lasers", J. Appl. Phys. 103(9), 094511 (2008)

52. David, C., et al.: LCLS/XPP experiments 10/2010. (to be published)

53. Quiney, H.M., Peele, A.G., Cai, Z., Paterson, D., Nugent, K.A.: "Diffractive imaging of highly focused X-ray fields", Nat. Phys. 2(2), 101-104 (2006)

54. Boutet, S, Williams, G.J.: "The Coherent X-ray Imaging (CXI) instrument at the Linac Coherent Light Source (LCLS)", New J. Phys. 12(3), 035024 (2010)

55. Yabashi, M., Hastings, J.B., Zolotorev, M.S., Mimura, H., Yumoto, H., Matsuyama, S., Yamauchi, K., Ishikawa, T.: "Single-Shot Spectrometry for X-Ray Free-Electron Lasers", Phys. Rev. Lett. 97(8), 084802 (2006)

56. Erko, A.: "Parallel X-ray fs-spectrometer", Seminar, European XFEL GmbH (March 2010)

57. Gahl, C., Azima, A., Beye, M., Deppe, M., Döbrich, K., Hasslinger, U., Hennies, F., Melnikov, A., Nagasono, M., Pietzsch, A., Wolf, M., Wurth, W., Föhlisch, A.: "A femtosecond X-ray/optical cross-correlator", Nat. Phot. 2, 165 (2008)

58. Rothhardt, J., Hädrich, S., Seise, E., Krebs, M., Tavella, F., Willner, A., Düsterer, S., Schlarb, H., Feldhaus, J., Limpert, J., Rossbach, J., Tünnermann, A.: "High average and peak power few-cycle laser pulses delivered by fiber pumped OPCPA system", Opt. Express 18(12), 12719-12726 (2010)

59. Thibault, P., Elser, V., Jacobsen, C., Shapiro, D., Sayre, D.: "Reconstruction of a yeast cell from X-ray diffraction data", Acta Cryst. A 62(4), 248-261 (2006)

60. Miao, J., Hodgson, K.O., Sayre, D.: "An approach to three-dimensional structures of biomolecules by using single-molecule diffraction images", Proc. Natl. Acad. Sci. USA 98(12), 6641-6645 (2001)

61. Sawhney, K.J.S., Alcock, S.G., Signorato, R.: "A novel adaptive bimorph focusing mirror and wavefront corrector with sub-nanometre dynamical figure control", Proc. SPIE 7803(1), 780303 (2010)